CELL BIOLOGY

CATSPERε extracellular domains are essential for sperm calcium channel assembly and activity modulation

Jae Yeon Hwang[1,2,3]*†, Huafeng Wang[1]†, Jong-Nam Oh[1], Jingon Kim[3], Sarah F. Finnegan[1], Niels E. Skakkebaek[4], Jean-Ju Chung[1,5]*

The sperm flagellar-specific CatSper Ca^{2+} channel is a multiprotein complex critical for successful fertilization. The four ancillary subunits, CATSPERβ, γ, δ, and ε, form a unique canopy structure over the pore-forming channel. However, how the canopy is formed and what it does in the assembled channel complex remain unknown. Here, we report that extracellular domains (ECDs) of CATSPERε are essential for canopy and holo-complex assembly and modulate channel activity during sperm capacitation. CATSPERε-deficient males are sterile due to the absence of the entire channel and defective sperm hyperactivation. Expressing ECD-truncated CATSPERε during spermatogenesis does not rescue the knockout because it fails to incorporate into the native complex. In contrast, addition of a CATSPERε ECD fragment during sperm capacitation significantly reduces sperm hyperactivation. These findings provide insight into the underlying molecular and developmental mechanisms of CatSper assembly and how the channel can be modulated in physiological settings and by therapeutic intervention.

INTRODUCTION

All living organisms enclosed by the plasma membrane communicate with the extracellular environment through membrane-associated proteins on their surface, such as membrane receptors and ion channels. The extracellular domains (ECDs) of these proteins are critical for sensing and transducing external signals into the cells. Typical examples are AMPA and *N*-methyl-D-aspartate (NMDA) receptors, where ligand binding to the ECDs triggers intracellular signaling (*1*, *2*). ECDs of various ion channels, including PIEZO1 and $Ca_v1.2$, often modulate ion conductance through the pore by undergoing conformational changes, thus participating in coordinating the opening or closing of the pore and influencing its activated or inactivated state (*3*, *4*). On the basis of the structural information and functional importance, recent studies have reported various drugs targeting these ECDs to modulate the activity of ion channels and receptors and the resulting downstream events (*5*). Notably, diazepam, which is used to treat anxiety and seizures, targets ECDs of γ-aminobutyric acid type A ($GABA_A$) receptors for its potentiation of γ-aminobutyric acid (GABA) response to suppress neuronal activity (*6*).

In mammalian spermatozoa, various membrane proteins are housed in the flagellar membrane for their navigation to successful fertilization in the female reproductive tract (*7*, *8*). Among them, the multiprotein CatSper Ca^{2+} channel complex presents the largest ECDs. Each of the four single transmembrane (TM) accessory subunits (CATSPERβ, γ, δ, and ε) interacts with one specific pore-forming subunit, forming a huge canopy structure over the heterotetrameric channel and linking the individual holo-complexes extracellularly in zigzag rows (*9*, *10*). CatSper-mediated Ca^{2+} signaling is critical for nearly all events in sperm capacitation (i.e., the collective process of acquiring fertility), including the development of hyperactivated motility and the acrosome reaction, and thus male fertility (*11*). However, our understanding of the physiological function of the CatSper canopy and the outcome of its intervention as a drug target remains largely unexplored.

Our previous study showed that CATSPERδ is required to maintain the stability of a pore-forming CATSPER1 subunit in developing male germ cells, suggesting its role in channel assembly (*12*). Recent advances in structural elucidation of the CatSper holo-complex and in situ higher-order arrangement further support that the canopy-forming subunits contribute not only to channel complex assembly but also potentially to activity regulation (*9*, *10*). Because the entire CatSper channel was absent in mature spermatozoa from *Catsperd*-null males (*12*), the detailed molecular mechanisms of assembly and the function of canopy ECDs in mature sperm remain unknown. This critical hurdle highlights the need for a different approach to further elucidate the physiological function of the canopy and individual TM subunits in mature spermatozoa. In the CatSper holo-complex, CATSPERε, paired with the CATSPER2 subunit (*9*), is located on the wing side of the CatSper zigzag rows (*10*) in the quadrilinear Ca^{2+} signaling nanodomains (*13*, *14*). Among the CatSper genes, human mutations in *CATSPERE* and its pairing partner *CATSPER2* have been reported more frequently (*15*, *16*), suggesting that their structural location is potentially vulnerable to cause functional defects in the CatSper channel and thus male infertility.

Here, using genetic and molecular dissection of CATSPERε, we show the molecular mechanisms of CATSPERε ECDs in channel complex assembly during germ cell development and their physiological function in mature spermatozoa. Genetic ablation of *Catspere* impairs sperm to develop hyperactivated motility as it leads to the absence of the entire CatSper complex, resulting in male infertility. Overexpression of the canopy roof–truncated CATSPERε prevents its interaction with other CatSper canopy-forming subunits in testicular germ cells. Last, we demonstrate that treatment of spermatozoa with a purified recombinant immunoglobulin (Ig)–like domain of CATSPERε ECDs during capacitation impairs sperm hyperactivation in vitro. These findings provide direct insights into the canopy function in CatSper complex assembly and activity regulation during sperm capacitation and suggest a strategy to target CatSper activity to control sperm fertility.

[1]Department of Cellular and Molecular Physiology, Yale School of Medicine, New Haven, CT, USA. [2]Department of Molecular Biology, Pusan National University, Busan, South Korea. [3]Department of Integrated Biological Science, Pusan National University, Busan, South Korea. [4]Department of Growth & Reproduction and EDMaRC, Rigshospitalet, University of Copenhagen, Copenhagen, Denmark. [5]Department of Obstetrics, Gynecology, and Reproductive Sciences, Yale School of Medicine, New Haven, CT, USA.
*Corresponding author. Email: jyhwang@pusan.ac.kr (J.Y.H.); jean-ju.chung@yale.edu (J.-J.C.)
†These authors contributed equally to this work.

RESULTS

CATSPERε is indispensable for sperm hyperactivation and male fertility

Four single-pass TM subunits (CATSPERβ, γ, δ, and ε) with their large ECDs form the canopy structure of the CatSper channel complex (*9*). The channel complexes are arranged in zigzag nanodomains along the sperm tail with CATSPERε uniquely positioned on the wing side (Fig. 1, A and B) (*10*). However, the detailed roles of CATSPERε and its physiological significance are currently unknown. Like other CatSper subunits, *CATSPERE* genes are expressed exclusively in the testis (Fig. 1C and fig. S1A), and CATSPERε protein is specifically localized to the flagellar membrane in the principal piece of human and mouse

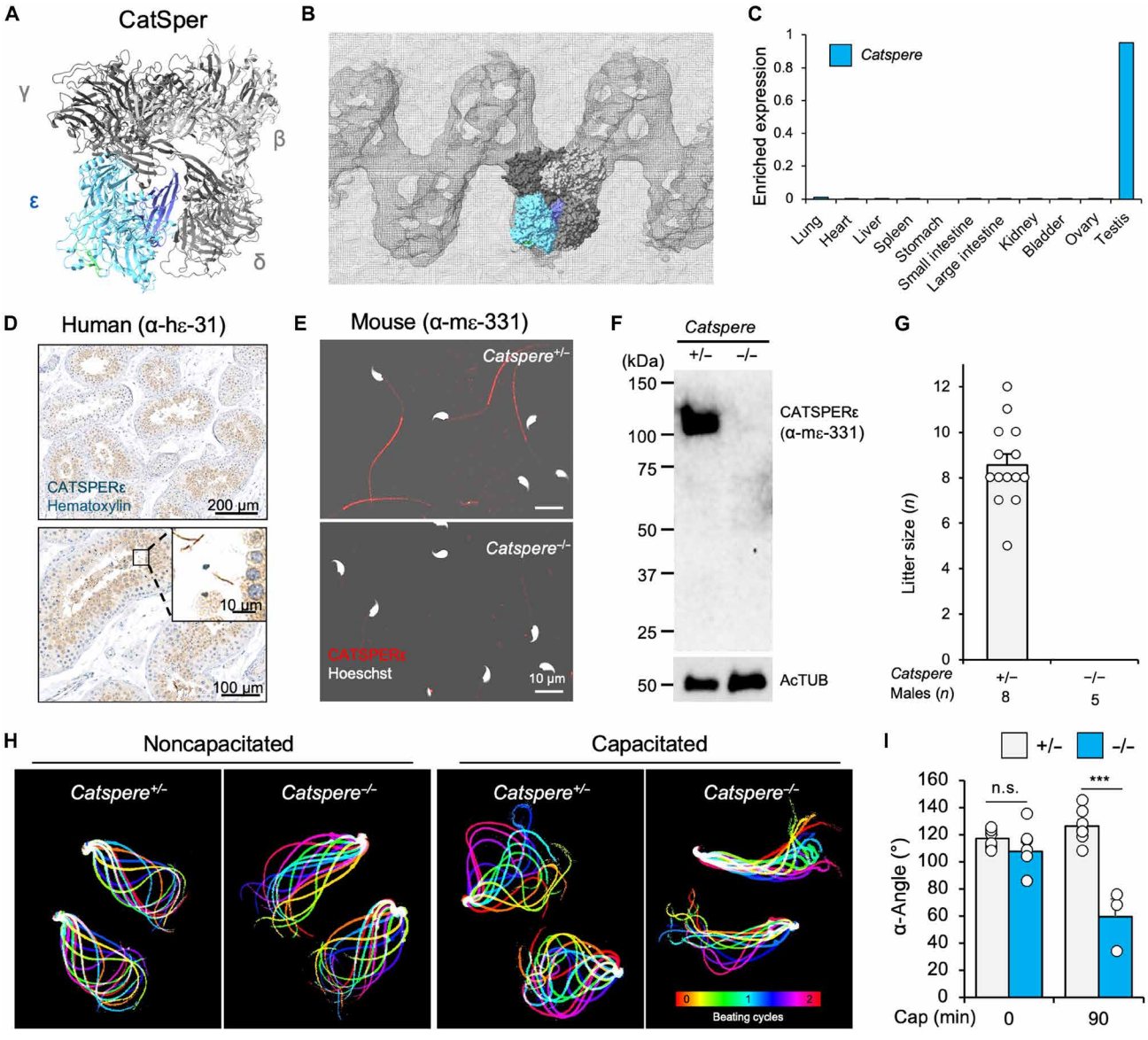

Fig. 1. The TM CATSPERε subunit is indispensable for sperm hyperactivation and male fertility. (**A** and **B**) Molecular position of CATSPERε within the atomic model and cryo–electron tomography (cryo-ET) map of the mouse CatSper complex. Shown are top-down views of CATSPERε (blue) in the single holo CatSper complex (A, PDB: 7EEB), fitted into the cryo-ET map of CatSper (B, EMDB: 24210). The epitope for α-CATSPERε (α-mε-331) that recognizes an ECD region (*40*) and the Ig-like domain are shown (green and light purple, respectively). (**C**) Tissue expression of *Catspere* mRNA. *Catspere* is specifically expressed in adult testis. (**D**) Immunostained CATSPERε in human testis. Human CATSPERε antibody (α-hε-31) (*13*) was used. Shown in the magnified inset (bottom) are testicular sperm. (**E**) CATSPERε in live epididymal sperm from heterozygous (+/−; top) and knockout (−/−; bottom) mice. Shown are merged images of fluorescence and corresponding differential interference contrast (DIC) images. DNA is stained with Hoechst. (**F**) Immunoblotting of CATSPERε in epididymal sperm from *Catspere*$^{+/-}$ and *Catspere*$^{-/-}$ (−/−) mice. Acetylated tubulin (AcTUB) is a loading control. (**G**) Litter sizes from fertile females mated with *Catspere*$^{+/-}$ or *Catspere*$^{-/-}$ males. Individual litter sizes are marked. (**H**) Flagellar waveform of the epididymal sperm from *Catspere*$^{+/-}$ and *Catspere*$^{-/-}$ mice before (left) and after (right) inducing capacitation. Sperm flagellar movements were recorded at a speed of 200 fps. The tail movements for two beating cycles are overlaid to show the waveform color coded in time. (**I**) Maximum angles of the primary flagellar curvature (α-angle) of the epididymal sperm. α-Angles of *Catspere*$^{+/-}$ (+/−, gray bars) and *Catspere*$^{-/-}$ (−/−, blue bars) sperm were measured before (0 min; +/−, 117.0° ± 2.9°; −/−, 107.6° ± 6.7°) and after (90 min; +/−, 126.2° ± 4.6°; −/−, 59.6° ± 12.8°) inducing capacitation (cap). n.s., not significant; ***$P < 0.001$. Data are represented as means ± SEM [(G) and (I)]. See also figs. S1 and S2.

spermatozoa (Fig. 1, D and E) (*13*). To understand the physiological significance of CATSPERε, we generated *Catspere*-null (*Catspere*$^{-/-}$) mice using CRISPR-Cas9 genome editing (fig. S2, A and B). By introducing two guide RNAs targeting the first and second exons, respectively, we obtained a null allele predicted to produce a frameshifted protein after the third amino acid. CATSPERε is absent in the testis and epididymal spermatozoa of *Catspere*$^{-/-}$ males (Fig. 1, E and F, and figs. S1B and S2C). *Catspere*$^{-/-}$ mice show no gross abnormalities in survival, appearance, or behavior, and null females are fertile. However, despite normal sperm production (fig. S2D), *Catspere*$^{-/-}$ males are completely infertile (Fig. 1G and fig. S2E), as are genetic disruptions of genes encoding other TM CatSper subunits (*11*, *12*, *17*–*20*). To understand how CATSPERε deficiency leads to male infertility, we examined sperm motility parameters using computer-assisted semen analysis (CASA). Curvilinear velocity (VCL) and amplitude of lateral head displacement (ALH) are significantly lower in sperm lacking CATSPERε after induction of capacitation (fig. S2F). Flagellar waveform analysis also revealed that sperm from *Catspere*$^{-/-}$ males fail to increase the maximum angle of the primary curvature in the midpiece (α-angle) and beat in an overall smaller envelope (Fig. 1, H and I), all indicative of defective sperm hyperactivation. These results demonstrate that CATSPERε deficiency impairs hyperactivated motility, resulting in male infertility.

Catspere-null sperm lack the entire CatSper channel, resulting in impaired Ca^{2+} signaling

To understand how genetic ablation of *Catspere* impairs sperm to develop hyperactivated motility, we examined whether the CatSper channel is present and functional in *Catspere*$^{-/-}$ sperm (Fig. 2). All CatSper subunits examined are absent in *Catspere*$^{-/-}$ sperm (Fig. 2, A and B), suggesting the lack of the entire CatSper channel, consistent with the observation in *Catsperd*$^{-/-}$ sperm (*12*). *Catspere*$^{-/-}$ sperm prematurely enhance capacitation-mediated tyrosine phosphorylation (pTyr) compared with wild-type (WT) sperm (Fig. 2C and fig. S2G), indicating impaired Ca^{2+} influx during capacitation (*21*). To directly test for defective Ca^{2+} influx through the CatSper channel, we performed electrophysiological recordings to measure the CatSper current ($I_{CatSper}$) in *Catspere*$^{-/-}$ spermatozoa (Fig. 2, D to F). When elicited under voltage ramp or step protocols, $I_{CatSper}$ is undetectable in *Catspere*$^{-/-}$ spermatozoa, indicating the absence of functional CatSper channels in spermatozoa. These results demonstrate that *Catspere*$^{-/-}$ spermatozoa lack the CatSper channel and therefore fail to transduce Ca^{2+} signals to develop hyperactivated motility during capacitation.

Truncated CATSPERε lacking the extracellular canopy roof does not interfere with the assembly of native full-length CATSPERε into the CatSper complex

The function of the unique large extracellular canopy above the pore-forming channel remains unknown. It could serve as a binding site for natural ligands, as a linker to multimerize the channels into a linear cooperative working unit, and/or as a chaperone to assemble the pore-forming tetramer in the specific counterclockwise order (*9*, *10*). Notably, sequence comparison analysis revealed that the C-terminal Ig-like domain and the stem region of CATSPERε are highly homologous to those of CATSPERδ (Fig. 3A) (*13*). In contrast to CATSPERβ and γ, which mediate intra- and interdimer interactions, respectively, CATSPERε and δ do not participate in the supramolecular interactions in the higher-order arrangement of the CatSper complexes (*10*). Thus, we hypothesized that this homology at the level of the canopy pole (Fig. 3B; i.e., the stem/pole and TM region only without the canopy roof) is more indicative of its function in channel assembly. To test this idea at the canopy pole and to further delineate the specific role of the canopy roof, we generated a transgenic mouse line overexpressing the roof-truncated, pole-retaining CATSPERε (i.e., truncated CATSPERε) specifically in the testis using the calmegin promoter (Fig. 3, A and B) (*22*, *23*).

The truncated CATSPERε is expressed in testis and is enriched in the microsomal fraction, indicating its membrane association (Fig. 3, C and D). However, the truncated protein is not detected in epididymal spermatozoa (Fig. 3, C and E). At the same time, the presence of the truncated CATSPERε in testis did not alter the typical quadrilinear localization of the CatSper channel in the principal piece of the mature sperm tail (Fig. 3, E and F). These results demonstrate that only the CatSper channel complexes assembled without the truncated CATSPERε are properly trafficked to the flagellar membrane. To test this idea, we first determined whether the truncated CATSPERε is complexed with other CatSper subunits. We performed coimmunoprecipitation using testis lysate (Fig. 3G). Native full-length CATSPERε and other examined CatSper subunits are detected in the CATSPERδ immunocomplex in the testis, independent of the transgene expression encoding the truncated CATSPERε. However, the immunocomplex of the truncated CATSPERε protein with anti–hemagglutinin (HA) antibody does not contain any CatSper subunits in the transgenic animal. This result demonstrates that, contrary to our hypothesis, the canopy pole is not sufficient to assemble the canopy structure but the roof-forming ECDs of CATSPERε are also necessary for the assembly of the CatSper channel holo-complex. Without this region, the truncated CATSPERε is retained in the cell body and progressively depleted in developing spermatids (Fig. 3H), supporting its absence in mature spermatozoa (Fig. 3, C and E) and minimal effect on the assembly of native CATSPERε into the CatSper complex (Fig. 3G). Accordingly, spermatozoa from the animal carrying both WT and transgenic alleles (WT; *TG*+) develop normal CatSper-mediated hyperactivated motility with normal pTyr after inducing capacitation (fig. S3, A and B). Also, protein levels of the native CatSper subunits are not altered in WT; *TG*+ spermatozoa (fig. S3, C and D).

The canopy roof–truncated CATSPERε fails to form heterotetrameric auxiliary complex in *Catspere*-knockout mice

In the absence of full-length CATSPERε, the truncated CATSPERε could replace the assembly function of native CATSPERε by incorporation into the CatSper complex while not being dominantly or equally in the presence of full-length CATSPERε (Fig. 3). To test this idea, we crossed the transgenic mice in the background of *Catspere*$^{-/-}$ mice to express only the transgene (*Catspere*$^{-/-}$; *TG*+; Fig. 4A). The truncated CATSPERε proteins are well expressed in the testis but not detected in the epididymal spermatozoa as observed in the spermatozoa of WT; *TG*+ males (Fig. 4A). CATSPERδ coimmunoprecipitation with testis lysate shows that truncated CATSPERε is not in complex with any of the native CatSper subunits examined, not even with the neighboring CATSPERδ or γ (Fig. 4B). This result demonstrates that the ECDs corresponding to the canopy roof of CATSPERε are indispensable for the assembly of all four auxiliary subunits into a fourfold complex via its interaction with CATSPERδ and γ.

Next, to understand how the CATSPERε truncation affects the assembly of the CatSper canopy and the entire CatSper complex, we

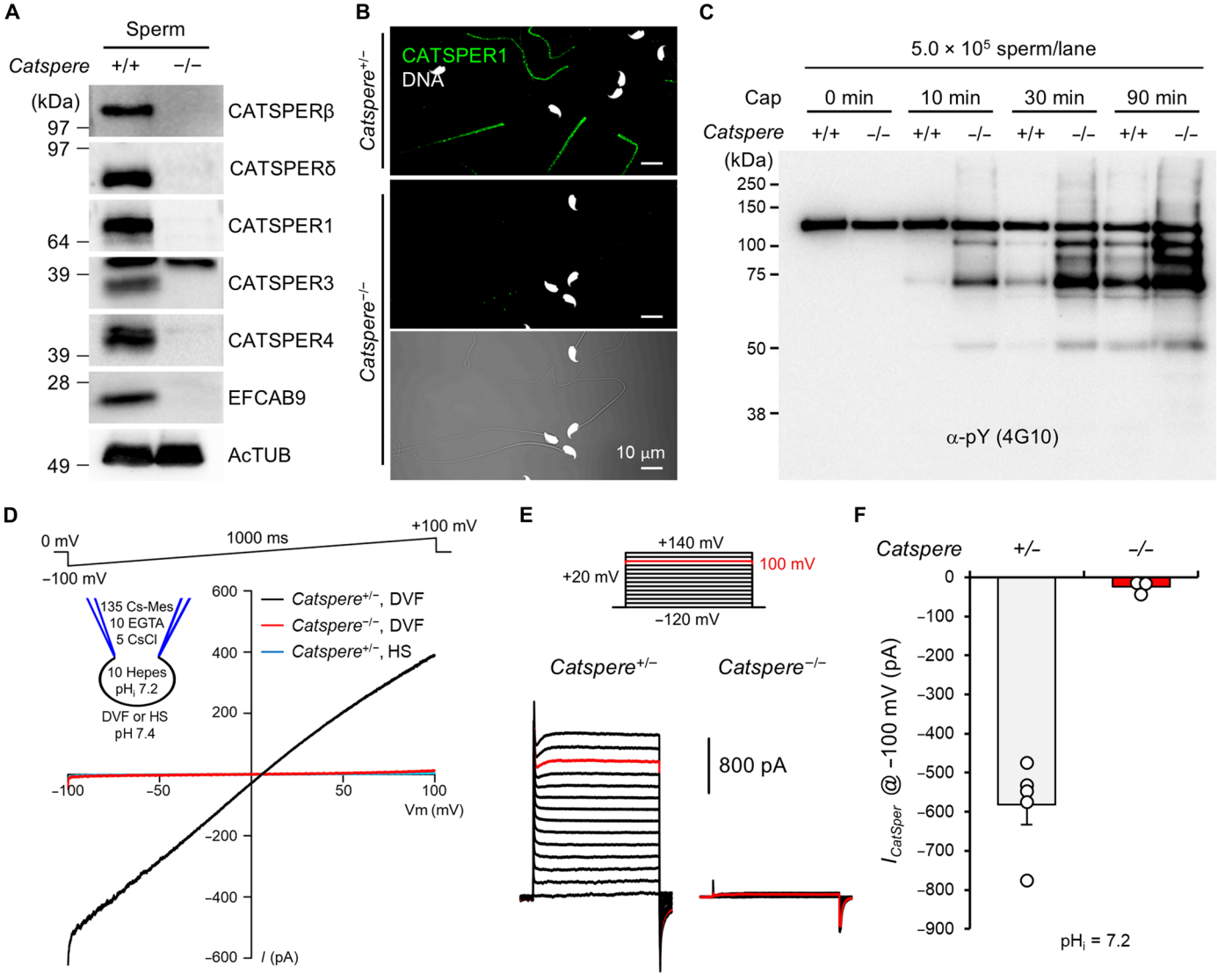

Fig. 2. *Catspere*-null spermatozoa lack a functional CatSper channel. (**A**) Immunoblotting of CatSper subunits in WT (+/+) and *Catspere*-null (−/−) epididymal sperm. Acetylated tubulin (AcTUB) is a loading control. (**B**) Confocal images of immunostained CATSPER1 in epididymal sperm from *Catspere*$^{+/-}$ (top) and *Catspere*$^{-/-}$ (middle and bottom) males. Fluorescence and corresponding DIC images are shown for *Catspere*$^{-/-}$ sperm (bottom). Hoechst is used for counterstaining DNA. (**C**) Immunoblotting of protein pTyr (pY) in sperm from WT (+/+) and *Catspere*-null (−/−) males. Time-course development of pY was examined for 90-min incubation of cauda epididymal sperm under capacitation (Cap) conditions. Protein extracts from the same number of sperm cells (5×10^5 cells per lane) were loaded per lane. (**D** and **E**) Representative traces of the CatSper current ($I_{CatSper}$) of corpus epididymal sperm from *Catspere*$^{+/-}$ and *Catspere*$^{-/-}$ males. $I_{CatSper}$ traces were elicited by a voltage-ramp protocol from a range of −100 to +100 mV with 0-mV holding potential (D) or by a step protocol from a range of −120 to +140 mV with 20-mV increments (E). A cartoon in (D) represents pH and ion composition (mM) in pipette solution and used bath solution for $I_{CatSper}$ measurement by voltage-ramp and step protocols. Divalent-free (DVF) solution or Hepes-buffered saline (HS) were used for bath solutions. (**F**) Inward $I_{CatSper}$ measured from *Catspere*$^{+/-}$ (gray, $n = 5$) and *Catspere*$^{-/-}$ (blue, $n = 3$) corpus sperm at −100 mV. Circles indicate the current from individual spermatozoa. Data are represented as means ± SEM. See also fig. S2.

analyzed the AlphaFold-predicted interactions of truncated CATSPERε with δ or γ (Fig. 4, C to E). In the predicted models, the intact CATSPERε ECDs interact normally with both δ and γ, and the predicted ε-δ and ε-γ dimers fit well into the atomic model of the CatSper canopy [CATSPERγ-β-δ-ε from Protein Data Bank (PDB): 7EEB] (Fig. 4, D and E). However, the truncated CATSPERε ECDs (i.e., the C-terminal Ig-like domain and stem region without the TM domain) are predicted to interact abnormally with these neighboring subunits, and the aberrant dimers do not fit the reported structure. Thus, the truncated roofless partial ECDs are likely to have altered their interaction with other canopy-forming auxiliary subunits, resulting in unsuccessful canopy assembly and canopy interactions with the pore-forming channel (CATSPER1-4-3-2).

The truncated CATSPERε fails to rescue impaired sperm hyperactivation by CATSPERε deficiency

Truncation of the canopy roof alters the interaction of CATSPERε with δ and γ, impairing ε incorporation into the canopy and thus into the entire CatSper channel complex (Figs. 3 and 4). In addition, the truncated CATSPERε appears to have little effect on the assembly and

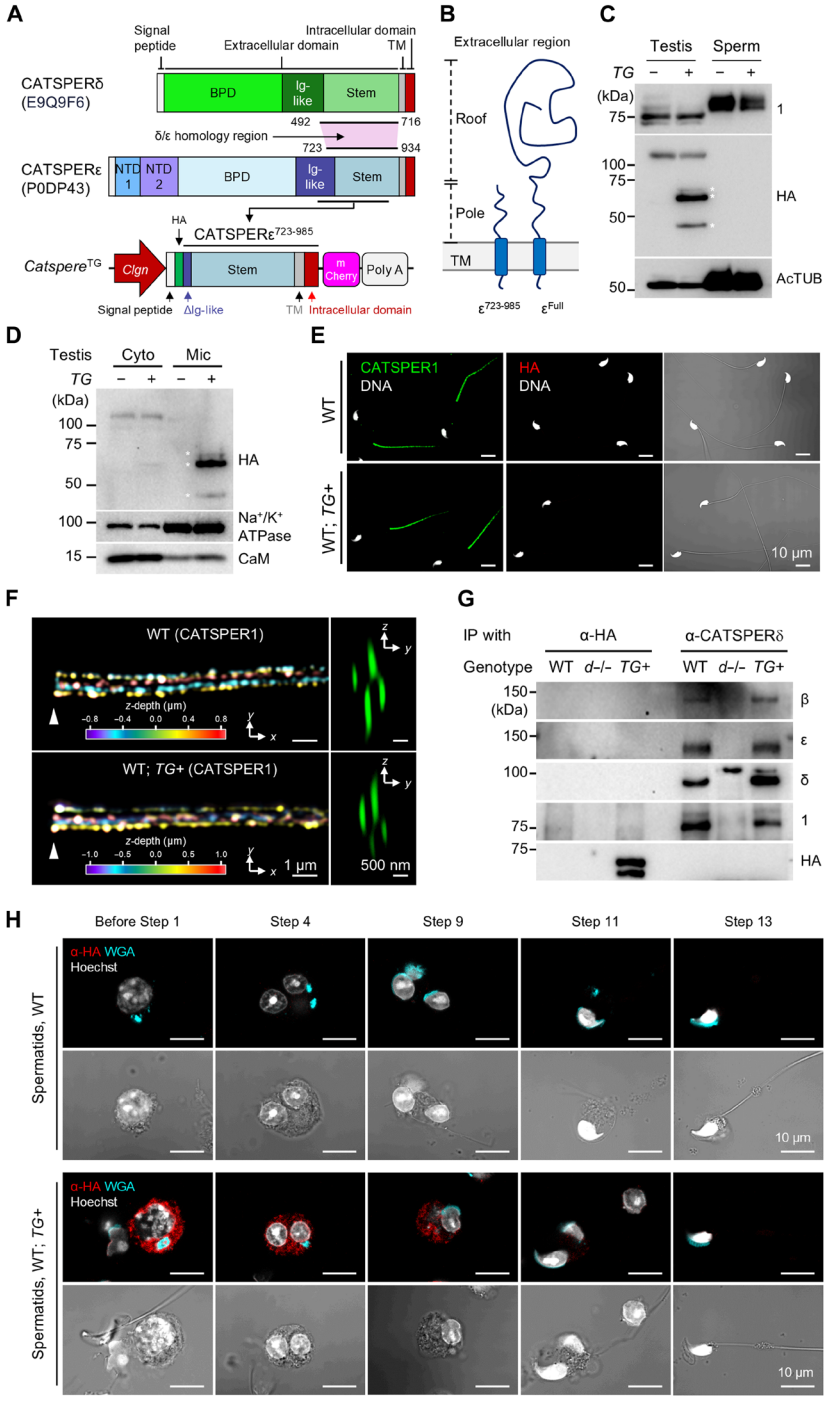

Fig. 3. Truncating the ECD hinders CATSPERε localization at the sperm flagella. (**A**) Diagram of the transgene (*Catspere*^{TG}) encoding a truncated CATSPERε ECD in mice. Shown is the domain organization of the mouse CATSPERε (UniProt: P0DP43) and CATSPERδ (UniProt: E9Q9F6). The transgene encodes the CATSPERδ-homologous region of CATSPERε fused to its native signal peptide and tags (~61 kDa), driven by the *Clgn* promoter for specific expression in testicular germ cells. (**B**) Topologies of the truncated ($\varepsilon^{723\text{-}985}$) and full-length ($\varepsilon^{Full}$) CATSPERε proteins. The truncated version retains only the canopy pole region. (**C**) Immunoblot of truncated CATSPERε in testis and sperm from *Catspere*$^{TG+}$ (*TG*+) mice. Proteins smaller than 50 kDa likely result from cleavage within the mCherry tag. Acetylated tubulin (AcTUB) serves as a loading control. (**D**) Immunoblot of truncated CATSPERε in cytosol and microsome fractions of testis from WT; *TG*+ males. Na^+/K^+ ATPase and calmodulin (CaM) are controls for fraction and loading. Asterisks (*) indicate the roof-truncated CATSPERε proteins. (**E**) Confocal images of immunostained CATSPER1 and HA in sperm. Merged fluorescence and corresponding DIC images (right) show HA-immunostained sperm. (**F**) 3D SIM images of immunostained CATSPER1 in sperm. *z*-depth is color coded (left), and *y*-*z* projections show cross sections (right). (**G**) Coimmunoprecipitation of native CatSper subunits and truncated CATSPERε in WT, *Catsperd*-null (*d*−/−), and WT; *Catspere*^{TG} (*TG*+) testis. (**H**) Confocal images of truncated CATSPERε in developing spermatids. Shown are fluorescence (top) and merged DIC and DNA fluorescence images (bottom). WGA stains sugar residues, and Hoechst counterstains DNA (E and H). The truncated CATSPERε is probed by α-HA [(C), (D), (E), (G), and (H)]. See also fig. S3.

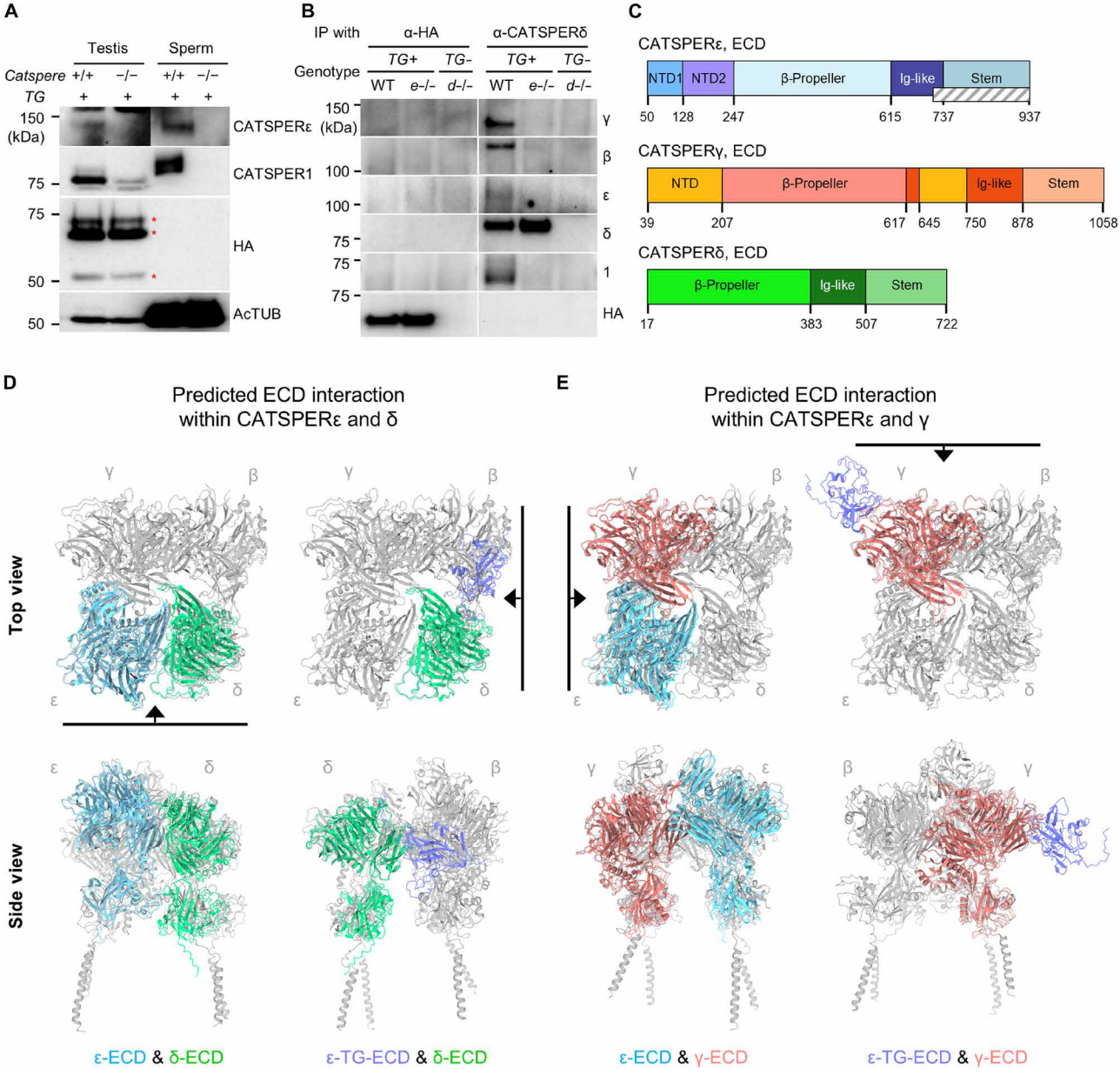

Fig. 4. Protein-protein interaction of the CATSPERε canopy with neighboring ancillary subunits is essential to assemble the entire CatSper channel complex. (**A**) Immunoblotting of truncated CATSPERε in testis and sperm from WT (+/+) and *Catspere*-null (−/−) males with the transgene (*TG*). Acetylated tubulin (AcTUB) is a loading control. Asterisks (*) indicate the roof-truncated CATSPERε expressed from the transgene. (**B**) Coimmunoprecipitation of the truncated CATSPERε and CatSper subunits in testis from WT and *Catspere*-null (*e*−/−) mice carrying the transgene (*TG*). α-HA was used to detect the truncated CATSPERε (A and B). *Catsperd*-null testis (*d*−/−) is used as a negative control. (**C**) Organization of CATSPERε, γ, and δ ECDs. Domain boundaries of each subunit are labeled. A gray sash in CATSPERε indicates the ECD region remaining in the truncated CATSPERε. (**D** and **E**) Predicted interaction of the truncated CATSPERε with CATSPERδ (D) or CATSPERγ (E). Shown are AlphaFold Multimer–predicted interaction of the whole (left) or truncated (right) CATSPERε ECD with whole ECDs of CATSPERδ (D) or CATSPERγ (E). Modeled structures for interacting two ECDs are fitted to the reference canopy structure of the CatSper channel colored in gray (PDB: 7EEB). Black lines marked in top view structures (top) indicate the orientation for the corresponding side views (bottom).

trafficking of the CatSper channel complex in the presence of native full-length CATSPERε in sperm from both WT and *Catspere*$^{+/-}$ males (figs. S3 and S4, A to F). Thus, we predict that *Catspere*$^{-/-}$; *TG*+ spermatozoa will lack a functional CatSper channel and will not rescue the physiological defects of *Catspere*$^{-/-}$ animals.

All CatSper subunits examined are absent in *Catspere*$^{-/-}$; *TG*+ spermatozoa (Fig. 5, A and B, and fig. S4F). Capacitated *Catspere*$^{-/-}$; *TG*+ spermatozoa aberrantly potentiate pTyr (fig. S4G), indicating impaired CatSper-mediated Ca^{2+} signaling. Electrophysiological recording shows that $I_{CatSper}$ is not detectable in *Catspere*$^{-/-}$; *TG*+ spermatozoa (Fig. 5, C to E), which is not significantly different from that recorded in *Catspere*$^{-/-}$ spermatozoa (Fig. 2, D to F). Although *Catspere*$^{-/-}$; *TG*+ males produce a comparable number of spermatozoa as heterozygous males (fig. S4H), they are infertile (Fig. 5F and fig. S4I)

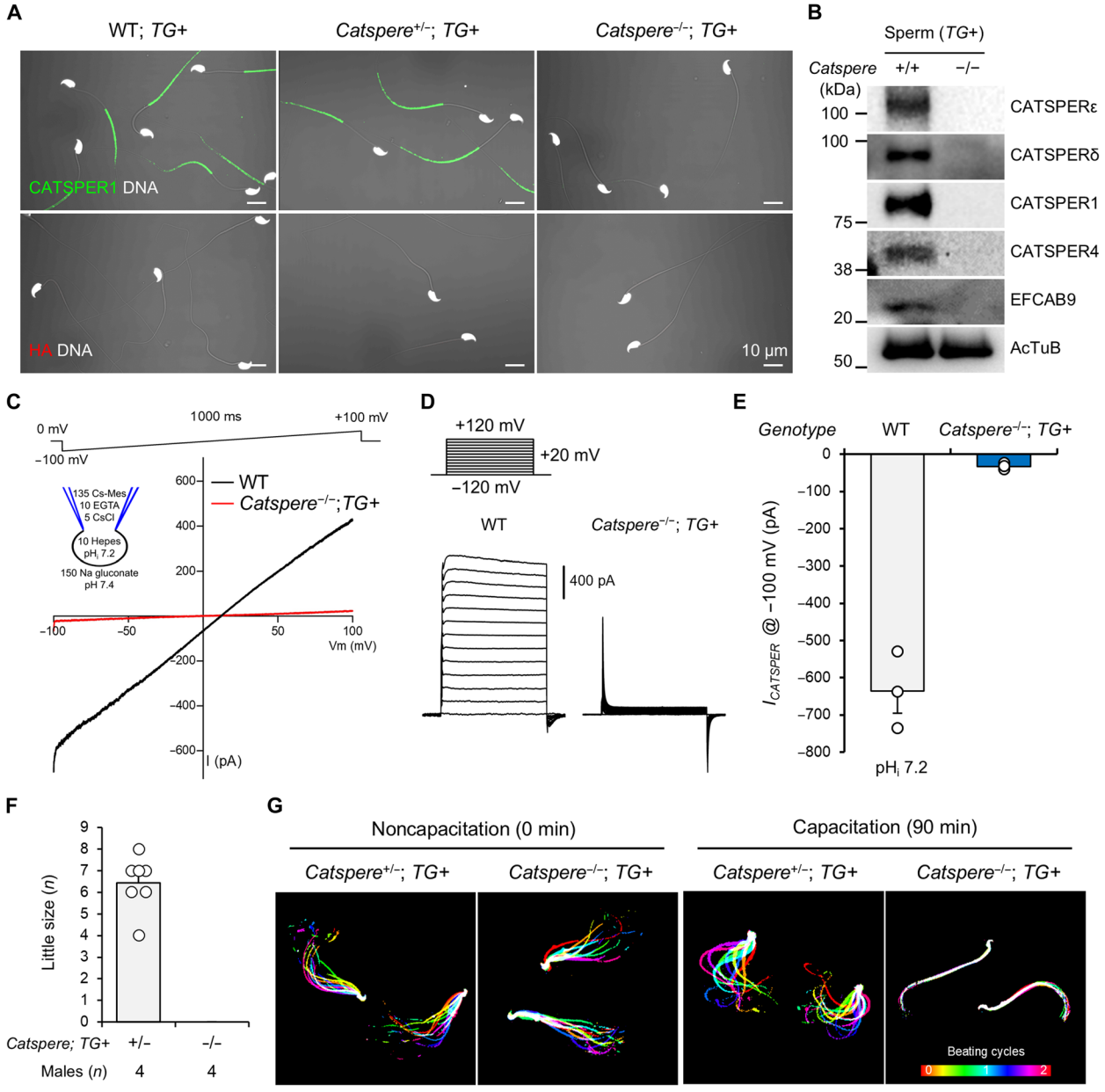

Fig. 5. ECD-truncated CATSPERε fails to rescue impaired sperm hyperactivation and male infertility in *Catspere*-null mice. (**A**) Confocal images of immunostained CATSPER1 and HA in epididymal sperm from WT, *Catspere*$^{+/-}$, and *Catspere*$^{-/-}$ mice crossed with the transgenic (*TG*) mice. Shown are merged views of fluorescence and corresponding DIC images. Hoechst is used to counterstain DNA. (**B**) Immunoblotting of CatSper subunits in epididymal sperm from WT and *Catspere*-null (*Catspere*−/−) males with the transgene (*TG*). Acetylated tubulin (AcTUB) is used as a loading control. (**C** and **D**) CatSper current ($I_{CatSper}$) of sperm from *Catspere*-null mice expressing the transgene (*Catspere*$^{-/-}$; *TG*+) and WT sperm. Shown are representative $I_{CatSper}$ traces elicited by ramp (C, −100 to +100 mV) and step (D, −120 to +140 mV, 20-mV increments) protocols. The holding potential for the voltage-ramp protocol and step protocol was 0 and −120 mV, respectively. A cartoon in (C) represents ion composition (mM) and pH in bath and pipette solution. (**E**) Comparison of the inward $I_{CatSper}$ of corpus WT sperm (gray bar, $N = 3$) and *Catspere*-null sperm with the transgene (*Catspere*$^{-/-}$; *TG*+, blue bar, $N = 3$) recorded at −100 mV. Circles indicate $I_{CatSper}$ measured from individual sperm. Data are represented as means ± SEM. (**F**) Litter size from pregnant females mated with *Catspere*+/− and *Catspere*−/− males carrying the transgene (*Catspere*$^{+/-}$; *TG*+ or *CatSpere*$^{-/-}$; *TG*+, respectively). Circles represent the number of pups from each litter. (**G**) Flagellar waveform of sperm from *Catspere*$^{+/-}$ and *Catspere*$^{-/-}$ mice expressing the transgene (*TG*+). Tail movements of head-tethered spermatozoa were recorded at 200 fps before (noncapacitated, 0 min; left) and after (capacitated, 90 min; right) incubation under capacitating conditions. Images for two beating cycles are overlaid and color coded in time. See also fig. S4.

with defective sperm hyperactivation (Fig. 5G and fig. S4J) like *Catspere*$^{-/-}$ males (Fig. 1). All these results demonstrate that *Catspere*$^{-/-}$; *TG*+ sperm lack the CatSper channel and that truncated CATSPERε cannot rescue male infertility caused by CATSPERε deficiency.

Ig-like domain of CATSPERε is critical in modulating CatSper activity and sperm hyperactivation

Our results using two *Catspere* genetic models provide strong evidence that the CATSPERε ECD regions that form the canopy roof are critical for their interaction with neighboring subunits to assemble the canopy and thus the CatSper channel holo-complex in developing male germ cells (Figs. 3 to 5). However, it remains to be determined whether and to what extent the canopy functions physiologically in mature spermatozoa, where the channel complexes are arranged in a higher order (*10*).

The Ig-like domain, present in all four canopy-forming subunits, mediates extensive interactions between them at the center of canopy roof, whereas the stem and TM domains do not (*9*). Consistently, among the individual ECDs of CATSPERε (i.e., N-terminal domain, β-propeller domain, and Ig-like), only the Ig-like domain is predicted to interact with the δ and γ ECDs at the canopy roof (fig. S5A), suggesting its importance in stabilizing the canopy structure. These structural characteristics suggest that changes in interaction mediated by the Ig-like domain could induce conformational changes in the canopy. Because each canopy subunit is paired with a pore-forming subunit via a TM interaction (*9*), conformational changes in the canopy, especially during capacitation, are likely to affect CatSper channel activity. Therefore, we hypothesize that treatment with a free Ig-like domain (CATSPERε$^{Ig\text{-}like}$; Fig. 6A), which is more soluble than other parts of CATSPERε (fig. S5, B and D), could interfere with the endogenous interactions, altering CatSper channel activity. To test this hypothesis and the specificity of the effect, we purified recombinant CATSPERε$^{Ig\text{-}like}$ proteins in WT and mutant forms (Fig. 6, B to E). In the mutant form, the amino acids predicted to interact with δ and γ ECDs were substituted with alanine (Fig. 6B and table S1) (*9*). To increase the solubility and purity of the recombinant proteins, we tagged the CATSPERε$^{Ig\text{-}like}$ proteins with thioredoxin (TrxA) and enhanced green fluorescent protein (EGFP) at the N and C termini, respectively (Fig. 6, C to E).

We found that incubating sperm under capacitating conditions in the presence of WT CATSPERε$^{Ig\text{-}like}$ protein (2 μg/ml; ~100 nM), but not mutant or tag proteins, reduced VCL and ALH by ~15% (Fig. 6F). Consistently, an ~70% reduction in hyperactivated motility was also observed with WT protein alone. These data suggest that the exogenous CATSPERε$^{Ig\text{-}like}$ protein interferes with protein-protein interactions at the canopy roof, thereby inhibiting CatSper function, and that this inhibition is reversed by mutating the interaction sites.

An aberrant increase in pTyr is an indication of the shortage of Ca^{2+} influx during capacitation, as shown by genetic ablation of CatSper or chelation of extracellular Ca^{2+} (*21*, *24*). However, inhibiting sperm hyperactivation by the WT protein is not accompanied by a pTyr increase (fig. S5D), suggesting its likely dynamic and/or transient interaction. In line with this, all recombinant proteins—WT and mutant CATSPERε$^{Ig\text{-}like}$, as well as the tag-only protein (tag)—remain associated with the surface of live sperm cells (fig. S5E), and the specific localization of the CATSPERε$^{Ig\text{-}like}$ proteins to the CatSper-residing principal piece was not detected (fig. S5F).

DISCUSSION

CatSper is a multiprotein channel complex composed of more than 10 TM subunits and three cytosolic components, arranged in higher-order zigzag rows (*11*). All reported TM subunit deficiencies in mice result in the absence of a functional CatSper channel in mature spermatozoa, leading to impaired male fertility due to the defective hyperactivation (*12*, *17*–*20*) despite the presence of all other CatSper subunits in the testis except the target protein (*13*, *14*, *17*, *25*). Thus, assembly defects at various steps from the assembly of individual holo-complexes (composed of canopy and pore-forming channels) to their higher-order zigzag arrangement can be attributed to the absence of functional CatSper channels in mature sperm from these TM knockout males (*12*, *17*, *25*). We have previously shown that CATSPERθ deficiency allows transient assembly of single holo-complexes, but results in defective interaction within CatSper dimers (*17*). The defective intradimer interaction prevents CatSper holo-complexes from exiting the cell body and trafficking to flagella of developing male germ cells (*17*). In contrast, the absence of either pore-forming or canopy-forming CatSper TM subunits fails to assemble transient CatSper holo-complexes in the testis (*12*, *25*). For example, CATSPER1 deficiency leads to incomplete organization of the pore-forming complex, whereas canopy-forming subunits are complexed in male germ cells (*12*, *25*). Deficiency of CATSPERδ or ε not only results in incomplete canopy assembly but also reduces the protein levels of the pore-forming subunits, presumably due to their altered stability (Fig. 4) (*12*). Thus, a deficiency of either pore-forming or canopy-forming TM subunits likely impairs the assembly of the CatSper holo-complexes during spermatogenesis, resulting in the absence of a functional channel in epididymal spermatozoa. However, considering the earlier mRNA expression of canopy-forming subunits than pore-forming subunits during development and their different interaction patterns and protein levels in the testis (*12*–*14*), a heterotetrameric canopy structure should form first, which presumably serves as a scaffold for 1:1 pairing with the pore-forming channels. Canopy roof–truncated CATSPERε cannot be incorporated into the CatSper complex (Fig. 4), highlighting the importance of the protein interactions between individual canopy TM subunits for functional CatSper channel assembly. Therefore, ECD-mediated canopy assembly may be another checkpoint to ensure a complete CatSper holo-complex for flagellar trafficking and functional expression in mature sperm.

Ion channel ECDs are important for the regulation of channel activity (*26*, *27*). Recent advances in cryo–electron microscopy (cryo-EM) techniques have revealed that ECDs undergo conformational changes during gating processes. For example, the ECD of GLIC, a proton-activated prokaryotic channel, is compacted and rotated counterclockwise by protonation, resulting in a widening of the pore region in the TM domains to evoke ion conductance (*28*). The protonated ECD of another pH-gating channel, TWIK1, closes the channel by sealing the top of the selectivity filter and suppresses K^+ conductance (*29*). The ligand-mediated conformational changes of the ECDs and the associated gating processes have also been reported for several neurotransmitter receptors. AMPA subunits are twisted by ligand binding, resulting in conformational changes of the gating ring at the ECDs and subsequent AMPA activation (*1*). Ligand binding to other heteropentameric Cys-loop family receptors, such as NMDA and glycine receptors, also induces rotation of the ECDs to propagate pore opening and channel activation (*2*, *30*). All these results show that channel activation is strongly associated with structural changes of ECDs. The current atomic structure of the

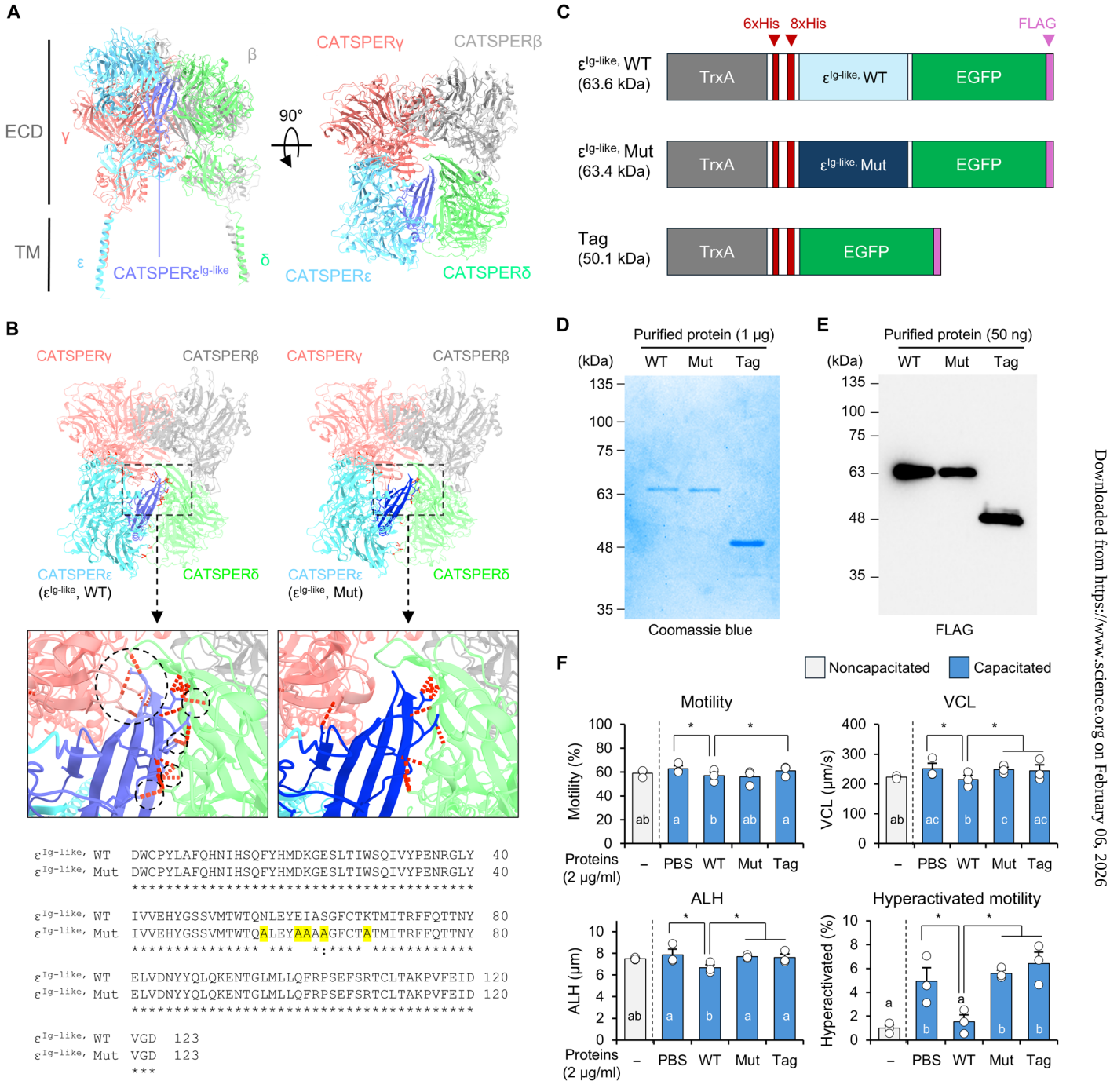

Fig. 6. Administration of the recombinant CATSPERε Ig-like domain protein attenuates sperm hyperactivation. (**A**) CATSPERε Ig-like domain in the canopy structure. Shown are the atomic model of CATSPERε, γ, δ, and β that form the canopy (left) and top view of the canopy structure (right) from PDB: 7EEB. Abbreviations: CATSPERε$^{Ig\text{-}like}$, CATSPERε Ig-like domain; ECD, extracellular domain; TM, transmembrane domain. (**B**) Predicted structure of the CATSPERε Ig-like domain interacting with CATSPERγ and CATSPERδ. Top-down views show the CatSper canopy with the WT (left) or mutant (right) CATSPERε Ig-like domain (ε$^{Ig\text{-}like}$). Insets detail the interaction interface, with predicted hydrogen bonds (red lines) between ε$^{Ig\text{-}like}$ and the ECDs of CATSPERγ and CATSPERδ. Black circles in the WT inset indicate absent hydrogen bonds in the mutant. Below is the amino acid sequence alignment of the WT and mutant ε$^{Ig\text{-}like}$ domain. Hydrogen bonds were predicted using a 1-Å threshold. (**C**) Diagram of recombinant WT and mutant CATSPERε$^{Ig\text{-}like}$ proteins (ε$^{Ig\text{-}like}$ WT and ε$^{Ig\text{-}like}$ Mut) fused with TrxA, EGFP, and FLAG and a tag-only protein (Tag). (**D** and **E**) Purified recombinant WT and mutant CATSPERε Ig-like domains. Shown are Coomassie blue–stained (D) and immunoblotted (E) recombinant proteins, probed by anti-DYKDDDDK. (**F**) Altered motility parameters of capacitated sperm incubated with the WT Ig-like domain of CATSPERε. The same volume of vehicle (PBS) was used for each group. CASA shows that WT CATSPERε$^{Ig\text{-}like}$ significantly reduces VCL, ALH, and hyperactivated motility in capacitated sperm compared to those incubated with mutant or Tag proteins. Sperm were capacitated for 90 min. *$P < 0.05$. Different letters within groups indicate significant differences. Data are represented as means ± SEM. See also fig. S5 and table S1.

CatSper holo-complex is a closed conformation resolved using the purified complex from testis and epididymis (*9*). Structural analyses revealed that the single TM domain of each canopy-forming subunit interacts with the S2 segment of the paired pore-forming subunit. In addition, their Ig-like domains interact with each other and stabilize the canopy structure at the roof just above the pore. Thus, the canopy structure connected to those of the neighboring channels might prevent the pore from opening and keep the channel in a closed conformation in noncapacitated sperm. Exogenous addition of purified recombinant WT CATSPERε Ig-like protein but not mutant protein inhibits sperm hyperactivation (Fig. 6). This result suggests that the recombinant Ig-like domain interferes with the interaction of the native CATSPERε ECD with those of the adjacent canopy-forming subunits, CATSPERγ and δ, and impairs the coordinated conformational changes of the canopy structure and/or supramolecular interaction of the zigzag arrangement during sperm capacitation. The absence of differences between WT and mutant proteins associated with the sperm surface, as well as the lack of detection of specific signals in the principal piece suggests that the bulky tags at the N and C termini likely prevents CATSPERε Ig-like from interacting stably and/or strongly with γ and δ at the canopy interface. Direct structural analysis of the capacitated sperm canopy will clarify how these interactions contribute to CatSper gating mechanisms.

Worldwide, more than 200 million pregnancies are unintended each year (*31*). Notably, more than 50% of unintended pregnancies eventually end in abortion, resulting in various health and social burdens for mothers and family members (*32*, *33*). Because of the negative consequences of unintended pregnancy, there is a growing awareness and demand for improved and/or diversified contraceptive methods. In particular, men currently have very limited options such as condoms and vasectomy. To this end, the recently reported plakogloblin-SPEM1 interaction inhibitor triptonide (*34*) and soluble adenylyl cyclase inhibitor TDI-11861 (*35*) are promising candidates for reversible male contraceptives that have been screened to target proteins specifically involved in spermiogenesis and sperm function, respectively.

CatSper is another good target validated for male fertility because of its specific expression and function in regulating sperm motility and fertility (*36*, *37*). However, the multicomponent organization and structural complexity of CatSper has hindered the development of CatSper-targeted contraceptives. The large volume of ECDs and the zigzag arrangement of the CatSper channels with a 180° rotation (*10*) suggest a uniquely high accessibility of the wing side of CATSPERε to potential biologics. Here, we show that treatment with a recombinant CATSPEREε Ig-like domain, which would disrupt the protein-protein interaction between CATSPERε and its neighbors CATSPERγ and δ within the holo-complex, inhibits CatSper and thus reduces sperm fertility (Fig. 6). Thus, small biologics and/or small molecules that specifically bind to CATSPERε ECDs could be potential strategies to intervene in CatSper function for the development of nonhormonal contraceptives.

MATERIALS AND METHODS

Animals

Catsper1 (RRID:MGI:3694476) and *Catspere*-null (RRID:MGI:5315771) mice (*12*, *20*) are maintained on a C57BL/6 background. WT C57BL/6 and CD1 mice were purchased from Charles River Laboratory and SamTako BioKorea (Osan, South Korea). Mice were managed in accordance with the guideline approved by the Yale Institute Animal Care and Use Committee (IACUC, #20079) and Pusan National University Institute of Animal Care and Use Committee (IACUC, #PNU-2025-0386).

Generation of Catspere-null and Catspere-TG mice and genotyping

Catspere-null mice were generated on a C57BL/6 background using a CRISPR-Cas9 system. Two guide RNAs, 5′-CGCCATGTTAGCCCGGCAGGTGG-3′ and 5′-AGAAGAACTGCAGCCTCCAGTGG-3′, in the *px330* vector were injected into the fertilized eggs collected from superovulated C57BL/6 females after mating with males. The developing two-cell embryos were transplanted into pseudopregnant CD1 females, and the founders' toe were biopsied for genotyping. Truncation of the target region was examined by genomic DNA (gDNA) polymerase chain reaction (PCR) using the F2 (5′-ACTGCCCTCGTTAGCTTTTTGTCA-3′) and R1 (5′-CCTCCTTGGGCAGTTGTAGTTCA-3′) primer pair. PCR products were Sanger sequenced, and female founders carrying the truncated allele were backcrossed with the WT males to examine germline transmission of the allele. The *Catspere*-null mice line with 63-kb gDNA deletion was maintained, and genotyping was performed by primer pairs of F2-R1 for the *Catspere*-null allele and F1 (5′- GCATACTAATTGCTTGGTCAAAAAC-3′)–R1 for the WT allele.

Transgenic mice were generated by introducing transgene encoding the truncated CATSPERε (*Catspere-TG*) in the *pClgn-mCherry* vector. Cloned *pClgn-Catspere-TG-mCherry* was linearized by restriction enzyme digestion and electroporated into the fertilized eggs collected from C57BL/6. The embryos were transplanted pseudopregnant CD1 females. Founders' toes were clipped for gDNA extraction. Extracted gDNAs were subjected for PCR with forward (5′-AAGATTTACAGGCAGTTTATTATTGAG-3′) and reverse (5′-GTCGGAGGGGAAGTTGGT-3′) primers. *Catspere-null*; *Catspere-TG* mice were generated by mating *Catspere-TG* male with WT background and *Catspere*-null females.

Human samples (BioBank)

Human materials for the present study were collected in accordance with the principles of the Declaration of Helsinki. The regional medical research ethics committee of the Capital Region of Copenhagen approved the use of human tissues stored in the biobank at the Department of Growth and Reproduction for gene expression studies (permit number H-16019636). All patients have given informed consent to donate their residual tissue for research.

Cell lines

Human embryonic kidney (HEK) 293T cells derived from human embryonic kidney (American Type Culture Collection; RRID:CVCL_0063) were cultured in Dulbecco's modified Eagle's medium (DMEM) (Gibco; catalog no. 11965092) supplemented with 10% fetal bovine serum (Gibco; catalog no. 10437028) and 1x Pen/Strep antibiotics (Gibco; catalog no. 15140-122) under the 37°C, 5% CO_2 condition. The cultured cells were used to test solubility of the recombinant proteins.

Bacterial strains

NEB 10-β bacterial strain (NEB; catalog no. C3019H) and DH5α bacterial strain (Enzynomics; catalog no. CP011) were used for molecular cloning. BL21-CodonPlus (DE3)-RIPL strain (Agilent; catalog no. 230280) was used for recombinant protein purification.

Mouse sperm preparation

Epididymal sperm from adult male mice were collected from caudal epididymis by swim-out in either M2 medium (EMD Millipore;

catalog no. MR-015-D) or Hepes saline (HS medium; 135 mM NaCl, 5 mM KCl, 1 mM $MgSO_4$, 2 mM $CaCl_2$, 20 mM Hepes, 5 mM glucose, 10 mM lactic acid, and 1 mM Na pyruvate; adjusted to pH 7.4). The collected epididymal sperm were incubated in human tubular fluid (HTF) medium (EMD Millipore; catalog no. MR-070-D) at a concentration of 2×10^6 cells/ml under the 37°C, 5% CO_2 condition for 90 min to induce capacitation.

Mouse testicular cell preparation

Dissociated mouse testicular cells were prepared as described previously (*25*, *38*). Briefly, seminiferous tubules in adult testes were dissociated mechanically after removing tunica albuginea. The tubules were washed with cold phosphate-buffered saline (PBS), chopped, and minced to dissociate testicular cells. The minced tubules in PBS were filtered with 40-μm mesh cell strainers to remove the debris. Filtered testicular cells were subjected to immunostaining.

Human testis section preparation

Human testis tissues were excised from the normal, tumor-free periphery of orchiectomy specimens from four adult patients with testicular germ cell cancer. Only the specimens with tumors typical of young adults, i.e., derived from germ cell neoplasia in situ (GCNIS), either seminoma or nonseminoma, were included. Excised specimens were immediately fixed in GR-fixative (7.4% formaldehyde; 4% acetic acid; 2% methanol; 0.57% sodium phosphate, dibasic; and 0.11% potassium phosphate, monobasic) for at least 16 hours. Samples were then dehydrated and embedded in paraffin.

Antibodies and reagents

Rabbit polyclonal anti-mouse CATSPER1 (*20*), 3, 4 (*18*), β (*39*), δ (*12*), EFCAB9 (*14*), and anti-human CATSPERε (α-hε-31) (*13*) were described previously.

Custom, in-house antibodies generated in this study

Rabbit polyclonal anti-mouse CATSPERε [α-mε-331; see also (*40*)] was generated by immunizing rabbits with the KLH-conjugated peptide (DGTVYLRTEDEFTKLDES) (Open Biosystems). Rabbit polyclonal anti-mouse CATSPERγ antibody (α-mγ-957) was generated by immunizing rabbits with the KLH-conjugated peptide (RDYTEEEIFRYNSPLDTTNSLI) (BioMatik). From the collected sera, the antibodies are affinity purified using the AminoLink coupling resin (Pierce). A hybridoma (clone 6D3) for a mouse monoclonal anti-CATSPER1 was created by immunizing mice with the purified N terminus of mouse CATSPER1 (1 to 150 amino acids) (GenScript). From the collected supernatant, the antibodies are affinity purified using the Protein G coupling resin.

Commercially available antibodies

Mouse monoclonal antibodies against HA (clone HA-7, H3663), acetylated tubulin (clone 6-11B-1, 7451), protein pTyr (clone 4G10, 05-321), and calmodulin (05-173) were from Sigma-Aldrich. Mouse monoclonal anti-Na^+/K^+ ATPase was from Santa Cruz Biotechnology (clone H-3, sc-48345). Rat monoclonal anti-DYKDDDDK was from Novus (clone L5, NBP1-06712). Rabbit monoclonal anti-HA (clone C29F4, 3724) was from Cell Signaling Technology. Goat anti-mouse (115-035-003), anti-rabbit (111-035-144), and anti-rat (112-035-167) IgG conjugated with horseradish peroxidase (HRP) were from Jackson ImmunoResearch. VeriBlot for immunoblotting of the coimmunoprecipitation was from Abcam (ab131366). Alexa Fluor 568–conjugated goat anti-mouse (A-11031), anti-rabbit (A-11036), anti-rat (A-11077) IgG (H+L), and Alexa Fluor 647–conjugated wheat germ agglutinin (WGA) (W32466) were from Invitrogen. Hoechst dye was from TOCRIS (5117) and Thermo Fisher Scientific (H1399). All other chemicals and reagents were from Sigma-Aldrich unless indicated.

Molecular cloning

A construct to generate *Catspere-TG* transgenic mice was cloned. Mouse *Catspere*, which is sequence-homologous to the mouse *Catsperd*, was subcloned into the *pClgn-mCherry* vector, gifted by M. Ikawa using the NEBuilder HiFi DNA Assembly Kit (NEB). Sequences encoding the native signaling peptide and HA tag are placed at the 5′ region of the *Catspere-TG* sequences. Codon-optimized sequences encoding WT and mutant CATSPERε$^{Ig\text{-}like}$ were synthesized from Thermo Fisher Scientific, which were subcloned into the *pET-32a*(+) vector using the NEBuilder HiFi DNA Assembly Kit (NEB). Constructs encoding fragments of the CATSPERε ECDs were subcloned into the phCMV3 vector using the NEBuilder HiFi DNA Assembly Kit (NEB).

Protein extraction and immunoblotting

Epididymal sperm

Whole sperm proteins were extracted as described previously (*25*). The collected sperm from cauda epididymis were washed with PBS followed by lysis using 2X lithium dodecyl sulfate (LDS) buffer for 10 min with vortexing at room temperature (RT). The lysates were centrifuged at 4°C, 18,000*g*, and supernatants were collected and denatured by incubation with 50 mM dithiothreitol (DTT) at 75°C for 10 min. The denatured sperm proteins were used for SDS–polyacrylamide gel electrophoresis (PAGE) and immunoblotting. Primary antibodies used are as follows: rabbit polyclonal anti-mouse CATSPERβ, CATSPERδ, CATSPER1, CATSPER3, CATSPER4, and EFCAB9 at 1 μg/ml, anti-mouse CATSPERε (1.6 μg/ml), rabbit monoclonal anti-HA (1:2000), and mouse monoclonal anti-pTyr (1:2000) and AcTUB (1:20,000).

Testis

Testis proteins were obtained as described previously (*25*). Testes were homogenized in 0.32 M sucrose buffer using a Dounce homogenizer and centrifuged at 4°C, 1000*g* for 15 min to discard the nucleus and debris. Collected supernatants were either lysed to 1X LDS buffer or subjected to centrifugation at 4°C, 100,000 rpm for 1 hour to separate the microsome and cytosolic fraction. Separated fractions were lysed to 2X LDS volume equivalently. Lysed testes samples were denatured by heating at 75°C for 2 or 10 min with 50 mM DTT supplement, followed by SDS-PAGE and immunoblotting. Primary antibodies for the immunoblotting were as follows: rabbit polyclonal anti-CATSPERε (2.4 μg/ml) and CATSPER1 (1 μg/ml), rabbit monoclonal anti-HA (1:2000), and mouse monoclonal anti-Na^+/K^+ ATPase (1:2000), CaM (1:2000), and AcTub (1:20,000). HRP-conjugated goat-anti mouse or rabbit antibodies were used for secondary antibody with a 1:20,000 concentration according to the host species of the primary antibody.

Transfected mammalian cells

Cultured 293T cells were transfected with HA-tagged recombinant CATSPERε ECDs using linear polyethylenimine (40 kDa, Polysciences). Cells were harvested after 36 to 48 hours from transfection followed by washing two times with PBS. The transfected cells were solubilized using 1% Triton X-100 in PBS for 4 hours at 4°C by gentle rocking and centrifuged at 4°C, 18,000*g* for 1 hour to pellet the insoluble fraction. Soluble proteins were mixed to 1x LDS buffer, and insoluble pellet fractions were lysed using 2X LDS buffer volume

equivalently. Proteins in LDS sample buffer were denatured by boiling at 75°C for 2 min with 50 μM DTT. Denatured samples were subjected to SDS-PAGE and immunoblotted using mouse anti-HA (1:2000) to probe recombinant CATSPERε ECD proteins.

Testis coimmunoprecipitation

Proteins in testes microsome were solubilized using PBS containing 1% Triton X-100 and cOmplete Mini, EDTA-free Protease Inhibitor Cocktail (Roche) at 4°C for 3 hours with gentle rocking. The lysates were centrifuged at 4°C, 18,000*g* for 1 hour, and supernatants with solubilized protein were collected. Solubilized microsome proteins were incubated with SureBeads Protein A Magenetic Beads (Bio-Rad) conjugated with rabbit polyclonal anti-CATSPERδ (0.5 μg) or mouse monoclonal anti-HA (0.5 μg) at 4°C overnight. The incubated magnetic beads were washed with 1% Triton X-100 in PBS, and the immunocomplexes were eluted with 2X LDS buffer containing 50 mM DTT, followed by heating at 75°C for 10 min. The elutes were used for SDS-PAGE and immunoblotting. Used primary antibodies are as follows: rabbit polyclonal anti-CATSPERγ, CATSPERδ, and CATSPER1 (1 μg/ml), CATSPERβ (2 μg/ml), CATSPERε (2.4 μg/ml), and rabbit monoclonal anti-HA (1:1000). VeriBlot (Abcam) was used for secondary antibody with a 1:200 to 1:500 concentration.

Immunocytochemistry

Fixed cell immunocytochemistry

The collected epididymal sperm and testicular germ cells were immunostained as described previously with minor modification (*25*, *38*). Briefly, epididymal sperm and dissociated testicular cells were washed with PBS and centrifuged at 700*g* for 5 min or at 250*g* for 3 min, respectively, to attach on the glass coverslips. For testicular cells, glass coverslips were coated with poly-D-lysine before centrifugation. The attached epididymal sperm and testicular cells were fixed with 4% paraformaldehyde (PFA) for 10 min at RT and washed three times with PBS. Fixed cells were permeablized by 0.1% Triton X-100 in PBS for 10 min followed by blocked with 10% normal goat serum in PBS for 1 hour at RT. Blocked samples on coverslips were incubated with primary antibodies at 4°C overnight. Primary antibodies used for the immunocytochemistry were as follows: rabbit polyclonal anti-CATSPER1 (10 μg/ml), rabbit monoclonal anti-HA (1:200), mouse monoclonal anti-pTyr (1:100). The samples were washed one time with 0.1% Triton X-100 in PBS and two times with PBS followed by incubation with goat anti-mouse or rabbit IgG conjugated with Alexa Fluor 568 (1:1000) in blocking solution for 1 hour at RT. Testicular cells were stained with WGA conjugated with Alexa Fluor 647 (0.1 μg/ml) together with secondary antibody. Immunostained coverslips were mounted with Vectashield (Vector Laboratories) and imaged using Plan-Apochrombat 63X/1.40 oil objective lens equipped in Zeiss LSM710 Elyra P1 (Invitrogen). Hoechst was used for counterstaining.

Live cell immunocytochemistry

Prepared sperm were incubated in M2 medium supplemented with the anti-mouse CATSPERε (20 μg/ml) at 37°C for 90 min. Sperm incubated with the primary antibody were washed with PBS followed by incubation with goat anti-rabbit IgG conjugated with Alexa Fluor 568 (1:1000) and Hoechst (1:500) in HS medium at 37°C for 30 min. Sperm were washed with PBS and placed on the glass coverslip coated with poly-D-lysine for 15 min followed by centrifugation at 700*g* for 5 min. Sperm were fixed with 4% PFA for 10 min at RT and washed three times with PBS. Prepared coverslips were mounted with ProLong Gold (Invitrogen) and imaged by a Plan-Apochrombat 63X/1.40 oil objective lens equipped in Zeiss LSM710 Elyra P1 (Invitrogen).

Immunohistochemistry

Immunohistochemistry was conducted by a standard indirect peroxidase method as described previously (*41*). Briefly, 4 μm tissue sections were subjected to heat-induced antigen retrieval using medical decloaking chamber (Biocare, Concord, CA, USA) in 0.01 M citrate buffer (pH 7.4) at 110°C for 30 min. Endogenous peroxidase was blocked with 1% H_2O_2 in methanol for 30 min, and the sections were blocked using 0.5% skimmed milk in Tris-buffered saline (TBS) for 30 min at RT. Sections were incubated with the anti-human CATSPERε antibody (*13*) diluted 1:75 in TBS overnight at 4°C and for 1 hour at RT in a humidified chamber. The slides incubated with the primary antibody were washed with TBS followed by incubation with anti-rabbit ImmPRESS HRP (peroxidase) antibody (Vector Laboratories, CA, USA) at RT for 30 min. After incubation with secondary antibody, slides were washed with TBS and visualized using ImmPACT DAB peroxidase (HRP) substrate (Vector Laboratories). The sections were subsequently counterstained with Mayer's hematoxylin and mounted with Aquatex mounting medium (Merck KGaA, Germany).

Recombinant CATSPERε$^{Ig\text{-}like}$ protein purification

Recombinant protein expression

Recombinant WT and mutant Ig-like domains of the CATSPERε tagged with TrxA at the N terminus and EGFP and FLAG at the C terminus and recombinant proteins carrying TrxA and EGFP-FLAG were obtained by a bacterial expression system as described previously (*14*, *42*). Briefly, constructs encoding recombinant proteins were transformed into the BL21-CodonPlus (DE3)-RIPL strain and starters were cultured in LB medium supplemented with ampicillin (100 μg/ml) and chloroamphenicol (25 μg/ml; KisanBio, Seoul, South Korea) at 37°C overnight. Saturated starters were inoculated fresh LB medium supplemented with antibiotics at a 1:50 ratio (v/v) and incubated at 37°C until OD_{600} (optical density at 600 nm) absorbance values of the cultivates reached to 0.4 to 0.7. The cultivates were treated with isopropyl-β-D-thiogalactopyranoside (IPTG; KisanBio) in a 1 mM final concentration to induce protein expression followed by incubation at 15°C for 14 to 16 hours.

Recombinant protein purification

Cultured bacteria to express recombinant proteins overnight were pelleted and lysed with phosphate-imidazole buffer (20 mM phosphate, 280 mM NaCl, 60 mM imidazole, and 0.5% Triton X-100, pH 7.4) supplemented with 1 mM DTT, 1 mM EGTA, and 1 mM phenylmethylsulfonyl fluoride (PMSF; Thermo Fisher Scientific) using sonication. Lysates were centrifuged at 16,000*g* at 4°C for 1 hour, and solubilized fractions in the supernatant were incubated with the HisPur Ni-NTA resin (Thermo Fisher Scientific) at 4°C for 30 min. Resins were serially washed with phosphate-imidazole buffer and 1X PBS and subjected to elution using 2X PBS supplemented with 300 mM imidazole, pH 7.4. Elutes were further incubated with Protein A/G PLUS-Agarose (Santa Cruz Biotechnology) cross-linked with the rat anti-DYKDDDDK monoclonal antibody (L5 clone; Novus) at 4°C overnight with gentle rocking. The agarose resin was washed with PBS and subjected to 0.1 M glycine (pH 2.3). The glycine elutes were buffer exchanged to PBS using a centrifugal concentrator (Satorius) and stored at 4°C until use.

Binding test of the recombinant CATSPERε$^{Ig\text{-}like}$ to epididymal sperm

Epididymal sperm were collected as described above and induced capacitation in HTF supplemented with recombinant WT CATSPERε$^{Ig\text{-}like}$, mutant CATSPERεIg-like, or tag protein or vehicle (PBS) (2 μg/ml) under the 37°C, 5% CO_2 condition for 90 min. Capacitated sperm incubated with recombinant proteins or vehicle were washed three times with PBS to remove unbound proteins. For immunoblotting, washed sperm were lysed as above and subjected to immunoblotting. Anti-DYKDDDDK (0.2 μg/ml) were used to detect FLAG-tagged recombinant proteins bound to capacitated sperm. Anti-pTyr (1:2000) were used to examine potentiation of global pTyr by altered Ca^{2+} influx. For immunostaining, washed sperm were attached to the glass coverslip and fixed with 4% PFA in PBS as described above. Fixed sperm were incubated with 0.1% Triton X-100 in PBS and blocked with 10% normal goat serum in PBS. Blocked coverslips were incubated with anti-DYKDDDK (2 μg/ml) in blocking buffer at 4°C overnight. The coverslips were washed with PBS and incubated with goat anti-rat IgG conjugate with Alexa Fluor 568 (1:1000) and Hoechst (1 μg/ml) for 1 hour at RT. Coverslips were washed with PBS and mounted using Vectashield and imaged using Plan-Apochromat 63x1.40 oil objective lens equipped in LSM900 (Carl Zeiss; NFEC-2025-01-302966).

Structural illumination microscopy

Mouse epididymal sperm on coverslips were immunostained as described above and subjected to three-dimensional (3D) structural illumination microscopy (SIM) imaging. 3D SIM imaging was performed with Zeiss LSM710 Elyra P1 using alpha Plan-APO 63X/1.40 oil objective lens (Carl Zeiss). *Z*-stack images was acquired with 100-nm intervals, and images of each section were taken using a laser at a 561-nm wavelength and five grid rotations with a 51-nm SIM grating period. Raw images were processed and rendered using Zen 2012 SP2 software (Carl Zeiss).

Histology analyses

Histological analyses of the mouse tissues were performed as described previously (*38*). Briefly, collected testes and epididymis were rinsed with PBS and fixed with 4% PFA in PBS at 4°C overnight. The fixed tissues were washed with PBS and serially dehydrated by incubation in ethanol to 100%. The tissues were embedded into paraffin followed by sectioning, and the tissue sections were deparaffinized to stain with hematoxylin and eosin (H&E). The stained sections were observed using a Nikon E200 microscope under 10x phase contrast objective (CFI Plan Achro 10X/0.25 pH1 WF, Nikon) and imaged by the equipped acA1300-200um complementary metal-oxide semiconductor (CMOS) camera (Basler AG).

Mating test

WT female mice were caged with *Catspere*$^{+/-}$, *Catsper*$^{-/-}$, *Catspere*$^{+/-}$; *TG*+, or *Catspere*$^{-/-}$; *TG*+ males and monitored for 2 months to record pregnancy and litter size.

Motility analysis

Flagella waveform analyses

Flagellar waveform analyses were carried out as described before (*43*, *44*). Briefly, noncapacitated or capacitated epididymal sperm (2×10^5 to 3×10^5 cells) were transferred to the 37°C HS and H-HTF medium, in fibronectin-coated Delta T chamber (Bioptechs). Planar flagellar movements of the head-tethered sperm were recorded for 2 s with 200 frames per second (fps) using a pco.edge sCMOS camera equipped in an Axio observer Z1 microscope (Carl Zeiss). Recorded images stacks were subjected to FIJI software (*45*) to measure the beating frequency and α-angle of the sperm tail (*12*) and to generate overlaid images to trace the waveform of sperm flagella as previously described (*13*).

Computer-assisted semen analysis

CASA was carried out as in previous studies (*25*, *44*, *46*). An aliquot of noncapacitated and capacitated sperm (3.0×10^6 cells/ml), which were incubated with or without recombinant proteins as above, was placed in a slide chamber (CellVision), and motility was examined on a 37°C stage of a Nikon E200 microscope under 10X phase contrast objective (CFI Plan Achro 10X/0.25 Ph1 BM, Nikon) equipped in a Nikon E200 microscope. Images were recorded at 50 fps using a CMOS video camera (Basler acA1300-200um, Basler AG, Ahrensburg, Germany) and analyzed by Sperm Class Analyzer (v6.3; Microptic, Barcelona, Spain). Over 200 motile sperm were analyzed for each trial, and at least three biological replicates were performed for each experimental group.

Electrophysiology

Whole sperm patch clamping was performed as described before (*25*). Sperm were collected from corpus epididymis and washed twice. Washed sperm were resuspended in HS medium followed by adhesion on a culture dish (Corning). Gigohm seals were formed at the cytoplasmic droplet of motile sperm (*47*). Cells were broken through by voltage stimulation (400 to 600 mV, 5 ms) and suction. Whole-cell CatSper currents were recorded in the divalent-free bath solution composed of 150 mM Na gluconate, 20 mM Hepes, and 5 mM Na_3HEDTA with pH 7.4 or HS medium (pH 7.4). Intrapipette solution for recording consisted of 135 mM $CsMeSO_3$, 5 mM CsCl, 10 mM EGTA, and 10 mM Hepes adjusted to pH 7.2. Data were sampled at 10 Hz and filtered at 1 kHz. The obtained current data were analyzed with Clampfit (v10.4, Axon, Gilze, The Netherlands) and plotted with Grapher (v8.8, Golden Software Inc., Golden, CO).

Tissue and testicular expression analyses

Transcript data of the CatSper subunits in adult mouse and human tissues were obtained from Mouse ENCODE transcriptome data (*48*) and HPA RNA-seq normal tissues dataset (*49*), respectively, at the National Center for Biotechnology Information (NCBI) (https://ncbi.nlm.nih.gov/gene/). Enriched tissue expression was calculated by normalizing the transcript level in each tissue with the sum of the transcript levels in the entire tissues. Enriched tissue expression levels of the CatSper subunits are shown as heatmap using GraphPad Prism 8.0 (GraphPad Software Inc., San Diego, CA).

Structural modeling and data analyses

A structure for the mouse CatSper complex was from the RCSC PDB (https://rcsb.org/; 7EEB). Protein structures were rendered and visualized by iCn3D at the NCBI (https://ncbi.nlm.nih.gov/Structure) (*50*). Dimer and trimer structures for ECDs of the CatSper auxiliary subunits and hydrogen bond formations of WT and mutant CATSPERε Ig-like domains were predicted using AlphaFold Multimer under the Google Colab notebook (*51*). UCSF ChimeraX (*52*) was used to visualize the atomic model of the CatSper channel (PDB: 7EEB) and to fit the predicted structures to the reference structure using a matchmaker tool incorporated in ChimeraX.

Statistical analyses

Statistical analyses were performed by the Student's *t* test. Differences were considered significant at $*P < 0.05$, $**P < 0.01$, and $***P < 0.001$.

Supplementary Materials

The PDF file includes:

Figs. S1 to S5

Legend for table S1

Other Supplementary Material for this manuscript includes the following:

Table S1

REFERENCES

1. S. Chen, Y. Zhao, Y. Wang, M. Shekhar, E. Tajkhorshid, E. Gouaux, Activation and desensitization mechanism of AMPA receptor-TARP complex by cryo-EM. *Cell* **170**, 1234–1246.e14 (2017).
2. T.-H. Chou, M. Epstein, R. G. Fritzemeier, N. S. Akins, S. Paladugu, E. Z. Ullman, D. C. Liotta, S. F. Traynelis, H. Furukawa, Molecular mechanism of ligand gating and opening of NMDA receptor. *Nature* **632**, 209–217 (2024).
3. S. Gao, X. Yao, J. Chen, G. Huang, X. Fan, L. Xue, Z. Li, T. Wu, Y. Zheng, J. Huang, X. Jin, Y. Wang, Z. Wang, Y. Yu, L. Liu, X. Pan, C. Song, N. Yan, Structural basis for human $Ca_v1.2$ inhibition by multiple drugs and the neurotoxin calciseptine. *Cell* **186**, 5363–5374.e16 (2023).
4. B. Xiao, Mechanisms of mechanotransduction and physiological roles of PIEZO channels. *Nat. Rev. Mol. Cell Biol.* **25**, 886–903 (2024).
5. J. Huang, X. Pan, N. Yan, Structural biology and molecular pharmacology of voltage-gated ion channels. *Nat. Rev. Mol. Cell Biol.* **25**, 904–925 (2024).
6. S. Zhu, C. M. Noviello, J. Teng, R. M. Walsh Jr., J. J. Kim, R. E. Hibbs, Structure of a human synaptic $GABA_A$ receptor. *Nature* **559**, 67–72 (2018).
7. D. Wachten, J. F. Jikeli, U. B. Kaupp, Sperm sensory signaling. *Cold Spring Harb. Perspect. Biol.* **9**, a028225 (2017).
8. H. Wang, L. L. McGoldrick, J.-J. Chung, Sperm ion channels and transporters in male fertility and infertility. *Nat. Rev. Urol.* **18**, 46–66 (2021).
9. S. Lin, M. Ke, Y. Zhang, Z. Yan, J. Wu, Structure of a mammalian sperm cation channel complex. *Nature* **595**, 746–750 (2021).
10. Y. Zhao, H. Wang, C. Wiesehoefer, N. B. Shah, E. Reetz, J. Y. Hwang, X. Huang, T.-e. Wang, P. V. Lishko, K. M. Davies, G. Wennemuth, D. Nicastro, J.-J. Chung, 3D structure and in situ arrangements of CatSper channel in the sperm flagellum. *Nat. Commun.* **13**, 3439 (2022).
11. J. Y. Hwang, J.-J. Chung, CatSper calcium channels: 20 years on. *Physiology* **38**, 125–140 (2023).
12. J.-J. L. Chung, B. Navarro, G. Krapivinsky, L. Krapivinsky, D. E. Clapham, A novel gene required for male fertility and functional CATSPER channel formation in spermatozoa. *Biophys. J.* **100**, 90a (2011).
13. J.-J. Chung, K. Miki, D. Kim, S.-H. Shim, H. F. Shi, J. Y. Hwang, X. Cai, Y. Iseri, X. Zhuang, D. E. Clapham, CatSperζ regulates the structural continuity of sperm Ca^{2+} signaling domains and is required for normal fertility. *Elife* **6**, e23082 (2017).
14. J. Y. Hwang, N. Mannowetz, Y. Zhang, R. A. Everley, S. P. Gygi, J. Bewersdorf, P. V. Lishko, J.-J. Chung, Dual sensing of physiologic pH and calcium by EFCAB9 regulates sperm motility. *Cell* **177**, 1480–1494.e19 (2019).
15. S. G. Brown, M. R. Miller, P. V. Lishko, D. H. Lester, S. J. Publicover, C. L. Barratt, S. Martins Da Silva, Homozygous in-frame deletion in CATSPERE in a man producing spermatozoa with loss of CatSper function and compromised fertilizing capacity. *Hum. Reprod.* **33**, 1812–1816 (2018).
16. S. Young, C. Schiffer, A. Wagner, J. Patz, A. Potapenko, L. Herrmann, V. Nordhoff, T. Pock, C. Krallmann, B. Stallmeyer, A. Röpke, M. Kierzek, C. Biagioni, T. Wang, L. Haalck, D. Deuster, J. N. Hansen, D. Wachten, B. Risse, H. M. Behre, S. Schlatt, S. Kliesch, F. Tüttelmann, C. Brenker, T. Strünker, Human fertilization in vivo and in vitro requires the CatSper channel to initiate sperm hyperactivation. *J. Clin. Invest.* **134**, e173564 (2024).
17. X. Huang, H. Miyata, H. Wang, G. Mori, R. Iida-Norita, M. Ikawa, R. Percudani, J.-J. Chung, A CUG-initiated CATSPERθ functions in the CatSper channel assembly and serves as a checkpoint for flagellar trafficking. *Proc. Natl. Acad. Sci. U.S.A.* **120**, e2304409120 (2023).
18. H. Qi, M. M. Moran, B. Navarro, J. A. Chong, G. Krapivinsky, L. Krapivinsky, Y. Kirichok, I. S. Ramsey, T. A. Quill, D. E. Clapham, All four CatSper ion channel proteins are required for male fertility and sperm cell hyperactivated motility. *Proc. Natl. Acad. Sci. U.S.A.* **104**, 1219–1223 (2007).
19. T. A. Quill, S. A. Sugden, K. L. Rossi, L. K. Doolittle, R. E. Hammer, D. L. Garbers, Hyperactivated sperm motility driven by CatSper2 is required for fertilization. *Proc. Natl. Acad. Sci. U.S.A.* **100**, 14869–14874 (2003).
20. D. Ren, B. Navarro, G. Perez, A. C. Jackson, S. Hsu, Q. Shi, J. L. Tilly, D. E. Clapham, A sperm ion channel required for sperm motility and male fertility. *Nature* **413**, 603–609 (2001).
21. J.-J. Chung, S.-H. Shim, R. A. Everley, S. P. Gygi, X. Zhuang, D. E. Clapham, Structurally distinct Ca^{2+} signaling domains of sperm flagella orchestrate tyrosine phosphorylation and motility. *Cell* **157**, 808–822 (2014).
22. M. Ikawa, T. Nakanishi, S. Yamada, I. Wada, K. Kominami, H. Tanaka, M. Nozaki, Y. Nishimune, M. Okabe, Calmegin is required for fertilin α/β heterodimerization and sperm fertility. *Dev. Biol.* **240**, 254–261 (2001).
23. D. Watanabe, M. Okabe, N. Hamajima, T. Morita, Y. Nishina, Y. Nishimune, Characterization of the testis-specific gene 'calmegin' promoter sequence and its activity defined by transgenic mouse experiments. *FEBS Lett.* **368**, 509–512 (1995).
24. F. A. Navarrete, F. A. García-Vázquez, A. Alvau, J. Escoffier, D. Krapf, C. Sánchez-Cárdenas, A. M. Salicioni, A. Darszon, P. E. Visconti, Biphasic role of calcium in mouse sperm capacitation signaling pathways. *J. Cell. Physiol.* **230**, 1758–1769 (2015).
25. J. Y. Hwang, H. Wang, Y. Lu, M. Ikawa, J.-J. Chung, *C2cd6*-encoded CatSperτ targets sperm calcium channel to Ca^{2+} signaling domains in the flagellar membrane. *Cell Rep.* **38**, 110226 (2022).
26. K. D. Nadezhdin, A. Neuberger, Y. A. Nikolaev, L. A. Murphy, E. O. Gracheva, S. N. Bagriantsev, A. I. Sobolevsky, Extracellular cap domain is an essential component of the TRPV1 gating mechanism. *Nat. Commun.* **12**, 2154 (2021).
27. L. Wang, H. Zhou, M. Zhang, W. Liu, T. Deng, Q. Zhao, Y. Li, J. Lei, X. Li, B. Xiao, Structure and mechanogating of the mammalian tactile channel PIEZO2. *Nature* **573**, 225–229 (2019).
28. N. Bharambe, Z. Li, D. Seiferth, A. M. Balakrishna, P. C. Biggin, S. Basak, Cryo-EM structures of prokaryotic ligand-gated ion channel GLIC provide insights into gating in a lipid environment. *Nat. Commun.* **15**, 2967 (2024).
29. T. S. Turney, V. Li, S. G. Brohawn, Structural basis for pH-gating of the K^+ channel TWIK1 at the selectivity filter. *Nat. Commun.* **13**, 3232 (2022).
30. X. Liu, W. Wang, Asymmetric gating of a human hetero-pentameric glycine receptor. *Nat. Commun.* **14**, 6377 (2023).
31. L. Nickels, W. Yan, Nonhormonal male contraceptive development—Strategies for progress. *Pharmacol. Rev.* **76**, 37–48 (2024).
32. J. Bearak, A. Popinchalk, B. Ganatra, A.-B. Moller, Ö. Tunçalp, C. Beavin, L. Kwok, L. Alkema, Unintended pregnancy and abortion by income, region, and the legal status of abortion: Estimates from a comprehensive model for 1990–2019. *Lancet Glob. Health* **8**, e1152–e1161 (2020).
33. S. Horvath, C. A. Schreiber, Unintended pregnancy, induced abortion, and mental health. *Curr. Psychiatry Rep.* **19**, 77 (2017).
34. Z. Chang, W. Qin, H. Zheng, K. Schegg, L. Han, X. Liu, Y. Wang, Z. Wang, H. McSwiggin, H. Peng, S. Yuan, J. Wu, Y. Wang, S. Zhu, Y. Jiang, H. Nie, Y. Tang, Y. Zhou, M. J. M. Hitchcock, Y. Tang, W. Yan, Triptonide is a reversible non-hormonal male contraceptive agent in mice and non-human primates. *Nat. Commun.* **12**, 1253 (2021).
35. M. Balbach, T. Rossetti, J. Ferreira, L. Ghanem, C. Ritagliati, R. W. Myers, D. J. Huggins, C. Steegborn, I. C. Miranda, P. T. Meinke, J. Buck, L. R. Levin, On-demand male contraception via acute inhibition of soluble adenylyl cyclase. *Nat. Commun.* **14**, 637 (2023).
36. K.-H. Lee, J. Y. Hwang, Ca^{2+} homeostasis and male fertility: A target for a new male contraceptive system. *Anim. Cells Syst.* **28**, 171–183 (2024).
37. N. A. Mariani, J. V. Silva, M. Fardilha, E. J. Silva, Advances in non-hormonal male contraception targeting sperm motility. *Hum. Reprod. Update* **29**, 545–569 (2023).
38. J. Y. Hwang, S. Nawaz, J. Choi, H. Wang, S. Hussain, M. Nawaz, F. Lopez-Giraldez, K. Jeong, W. Dong, J.-N. Oh, K. Bilguvar, S. Mane, C.-K. Lee, C. Bystroff, R. P. Lifton, W. Ahmad, J.-J. Chung, Genetic defects in *DNAH2* underlie male infertility with multiple morphological abnormalities of the sperm flagella in humans and mice. *Front. Cell Dev. Biol.* **9**, 662903 (2021).
39. J. Liu, J. Xia, K.-H. Cho, D. E. Clapham, D. Ren, CatSperβ, a novel transmembrane protein in the CatSper channel complex. *J. Biol. Chem.* **282**, 18945–18952 (2007).
40. K. Nand, T. B. Jordan, X. Yuan, D. A. Basore, D. Zagorevski, C. Clarke, G. Werner, J. Hwang, H. Wang, J. Chung, A. McKenna, M. D. Jarvis, G. Singh, C. Bystroff, Bacterial production of recombinant contraceptive vaccine antigen from CatSper displayed on a human papilloma virus-like particle. *Vaccine* **41**, 6791–6801 (2023).
41. J. E. Nielsen, A. D. Rolland, E. Rajpert-De Meyts, C. Janfelt, A. Jørgensen, S. B. Winge, D. M. Kristensen, A. Juul, F. Chalmel, B. Jégou, Characterisation and localisation of the endocannabinoid system components in the adult human testis. *Sci. Rep.* **9**, 12866 (2019).
42. J. Kim, J. Y. Hwang, Intracellular domain of CATSPER1 could serve as a cytoplasmic platform for redox processes in mammalian sperm. *Anim. Biosci.* **38**, 655–664 (2025).
43. J. Y. Hwang, J. Maziarz, G. P. Wagner, J.-J. Chung, Molecular evolution of CatSper in mammals and function of sperm hyperactivation in gray short-tailed opossum. *Cells* **10**, 1047 (2021).

44. H. Wang, Q. Dou, K. J. Jeong, J. Choi, V. N. Gladyshev, J.-J. Chung, Redox regulation by TXNRD3 during epididymal maturation underlies capacitation-associated mitochondrial activity and sperm motility in mice. *J. Biol. Chem.* **298**, 102077 (2022).
45. J. Schindelin, I. Arganda-Carreras, E. Frise, V. Kaynig, M. Longair, T. Pietzsch, S. Preibisch, C. Rueden, S. Saalfeld, B. Schmid, J. Y. Tinevez, D. J. White, V. Hartenstein, K. Eliceiri, P. Tomancak, A. Cardona, Fiji: An open-source platform for biological-image analysis. *Nat. Methods* **9**, 676–682 (2012).
46. J. Y. Hwang, Analysis of Ca^{2+}-mediated sperm motility to evaluate the functional normality of the sperm-specific Ca^{2+} channel, CatSper. *Front. Cell Dev. Biol.* **12**, 1284988 (2024).
47. Y. Kirichok, B. Navarro, D. E. Clapham, Whole-cell patch-clamp measurements of spermatozoa reveal an alkaline-activated Ca^{2+} channel. *Nature* **439**, 737–740 (2006).
48. F. Yue, Y. Cheng, A. Breschi, J. Vierstra, W. Wu, T. Ryba, R. Sandstrom, Z. Ma, C. Davis, B. D. Pope, Y. Shen, D. D. Pervouchine, S. Djebali, R. E. Thurman, R. Kaul, E. Rynes, A. Kirilusha, G. K. Marinov, B. A. Williams, D. Trout, H. Amrhein, K. Fisher-Aylor, I. Antoshechkin, G. DeSalvo, L. H. See, M. Fastuca, J. Drenkow, C. Zaleski, A. Dobin, P. Prieto, J. Lagarde, G. Bussotti, A. Tanzer, O. Denas, K. Li, M. A. Bender, M. Zhang, R. Byron, M. T. Groudine, D. McCleary, L. Pham, Z. Ye, S. Kuan, L. Edsall, Y. C. Wu, M. D. Rasmussen, M. S. Bansal, M. Kellis, C. A. Keller, C. S. Morrissey, T. Mishra, D. Jain, N. Dogan, R. S. Harris, P. Cayting, T. Kawli, A. P. Boyle, G. Euskirchen, A. Kundaje, S. Lin, Y. Lin, C. Jansen, V. S. Malladi, M. S. Cline, D. T. Erickson, V. M. Kirkup, K. Learned, C. A. Sloan, K. R. Rosenbloom, B. Lacerda de Sousa, K. Beal, M. Pignatelli, P. Flicek, J. Lian, T. Kahveci, D. Lee, W. J. Kent, M. Ramalho Santos, J. Herrero, C. Notredame, A. Johnson, S. Vong, K. Lee, D. Bates, F. Neri, M. Diegel, T. Canfield, P. J. Sabo, M. S. Wilken, T. A. Reh, E. Giste, A. Shafer, T. Kutyavin, E. Haugen, D. Dunn, A. P. Reynolds, S. Neph, R. Humbert, R. S. Hansen, M. de Bruijn, L. Selleri, A. Rudensky, S. Josefowicz, R. Samstein, E. E. Eichler, S. H. Orkin, D. Levasseur, T. Papayannopoulou, K. H. Chang, A. Skoultchi, S. Gosh, C. Disteche, P. Treuting, Y. Wang, M. J. Weiss, G. A. Blobel, X. Cao, S. Zhong, T. Wang, P. J. Good, R. F. Lowdon, L. B. Adams, X. Q. Zhou, M. J. Pazin, E. A. Feingold, B. Wold, J. Taylor, A. Mortazavi, S. M. Weissman, J. A. Stamatoyannopoulos, M. P. Snyder, R. Guigo, T. R. Gingeras, D. M. Gilbert, R. C. Hardison, M. A. Beer, B. Ren, Mouse ENCODE Consortium, A comparative encyclopedia of DNA elements in the mouse genome. *Nature* **515**, 355–364 (2014).
49. L. Fagerberg, B. M. Hallström, P. Oksvold, C. Kampf, D. Djureinovic, J. Odeberg, M. Habuka, S. Tahmasebpoor, A. Danielsson, K. Edlund, A. Asplund, E. Sjöstedt, E. Lundberg, C. A. Szigyarto, M. Skogs, J. O. Takanen, H. Berling, H. Tegel, J. Mulder, P. Nilsson, J. M. Schwenk, C. Lindskog, F. Danielsson, A. Mardinoglu, A. Sivertsson, K. von Feilitzen, M. Forsberg, M. Zwahlen, I. Olsson, S. Navani, M. Huss, J. Nielsen, F. Ponten, M. Uhlén, Analysis of the human tissue-specific expression by genome-wide integration of transcriptomics and antibody-based proteomics. *Mol. Cell. Proteomics* **13**, 397–406 (2014).
50. J. Wang, P. Youkharibache, D. Zhang, C. J. Lanczycki, R. C. Geer, T. Madej, L. Phan, M. Ward, S. Lu, G. H. Marchler, Y. Wang, S. H. Bryant, L. Y. Geer, A. Marchler-Bauer, iCn3D, a web-based 3D viewer for sharing 1D/2D/3D representations of biomolecular structures. *Bioinformatics* **36**, 131–135 (2020).
51. R. Evans, M. O'Neill, A. Pritzel, N. Antropova, A. Senior, T. Green, A. Žídek, R. Bates, S. Blackwell, J. Yim, Protein complex prediction with AlphaFold-Multimer. bioRxiv 463034 [Preprint] (2021). https://doi.org/10.1101/2021.10.04.463034.
52. E. C. Meng, T. D. Goddard, E. F. Pettersen, G. S. Couch, Z. J. Pearson, J. H. Morris, T. E. Ferrin, UCSF ChimeraX: Tools for structure building and analysis. *Protein Sci.* **32**, e4792 (2023).

Acknowledgments: We thank M. Ikawa at Osaka University for sharing the *pCIgn-mCherry* vector, G. Clouser for helping with mouse maintenance and antibody characterization, M. Raju and N. Lang for helping with initial characterization of waveform analysis of WT; *TG+* sperm, S. B. Winge at Copenhagen University Hospital for supporting human histology sample preparation, X. Huang and C. Gardner at Yale School of Medicine for supporting initial revision experiments, and J. Kim and J. Y. Lee at Pusan National University for supporting protein purification. J.Y.H. was a recipient of a Male Contraceptive Initiative postdoctoral fellowship. **Funding:** This work was supported by the National Institutes of Health R01HD096745 (J.-J.C.); Male Contraceptive Initiative David Sokal award (J.-J.C.); Blavatnik Innovation Fund (J.-J.C.); National Research Foundation, MSIT, South Korea RS-2024-00351076 (J.Y.H.); and National Research Foundation, MSIT, South Korea RS-2024-00399681 (J.Y.H.). **Author contributions:** Conceptualization: J.Y.H., H.W., and J.-J.C. Methodology: J.Y.H., H.W., and N.E.S. Software: H.W. Validation: J.Y.H., H.W., and S.F.F. Formal analysis: J.Y.H., H.W., J.-N.O., N.E.S., and J.-J.C. Investigation: J.Y.H., H.W., J.-N.O., J.K., and S.F.F. Resource: J.Y.H. and J.-J.C. Data curation: J.Y.H., H.W., J.K., and J.-J.C. Writing—original draft: J.Y.H. and J.-J.C. Writing—review and editing: J.Y.H. and J.-J.C. Visualization: J.Y.H. and J.-N.O. Supervision: J.Y.H. and J.-J.C. Project administration: J.Y.H. and J.-J.C. Funding acquisition: J.Y.H. and J.-J.C. **Competing interests:** The authors declare that they have no competing interests. **Data and materials availability:** All data and code needed to evaluate and reproduce the results in the paper are present in the paper and/or the Supplementary Materials.

Submitted 28 January 2025
Accepted 2 January 2026
Published 28 January 2026
10.1126/sciadv.adw3414

ScienceAdvances

CATSPER# extracellular domains are essential for sperm calcium channel assembly and activity modulation

Jae Yeon Hwang, Huafeng Wang, Jong-Nam Oh, Jingon Kim, Sarah F. Finnegan, Niels E. Skakkebaek, and Jean-Ju Chung

Sci. Adv. **12** (5), eadw3414. DOI: 10.1126/sciadv.adw3414

Science Advances (ISSN 2375-2548) is published by the American Association for the Advancement of Science. 1200 New York Avenue NW, Washington, DC 20005. The title *Science Advances* is a registered trademark of AAAS.